

The Probe of Inflation and Cosmic Origins

A Space Mission Study Report
December, 2018

Principal Investigator:

Steering Committee:

Executive Committee:

Contributors:

Endorsers:

1 Executive Summary (2 pg, Hanany)

48 remaining pages are distributed 29/19: 29 pages for science (including foregrounds and systematics), 19 for instrument, technology, mission, management and cost.

2 Science

2.1 Introduction (1.5 pgs)

Theoretical development and measurements of the cosmic microwave background radiation (PICO) over the last decade have uncovered tremendous potential for new discoveries over the next 10-20 years. The new discoveries are promising to be no less revolutionary than those attained through the CMB to date.

Fluctuations of the space-time metric during the epoch of inflation, near the Planck time, have generated gravitational waves that embed a unique ‘B-mode’ signature on the polarization of the CMB. A detection of the signal “would be a watershed discovery”, a quote from the 2010 decadal panel report, as it would be our first signal from the epoch of quantum gravity at the beginning of the Universe. The signal would also give strong clues about the nature of inflation. An intense hunt for the signal is ongoing by sub-orbital instruments. These searches have already ruled out several models for the inflaton potential. But the measurements, by the *Planck* space mission and other sub-orbital experiments, have also revealed that emission by our own galaxy is a source of confusion that must be separated with high fidelity before definitive discovery, or stronger upper limits, can be claimed. PICO is poised to detect or place unprecedented constraints on the inflationary-induced B-mode signal.

(SAY SOMETHING ABOUT CONSTRAINING MODELS OF REIONIZATION, INTRODUCE TAU; NEED TAU IN THE NEXT PARAGRAPH - Nick / Colin?)

Lensing of the CMB photons by structures as they traverse the Universe provides a projected map of all the matter in the universe from the epoch of decoupling until today. The non-zero mass of neutrinos affects the clustering of matter and thus can in principle be inferred from maps of the projected matter. However, the precision of determining the neutrino mass scale, using the CMB or *any* other cosmological probe, is limited by knowledge of the optical depth to reionization, τ . (EXPLAIN WHY IN 1-2 SENTENCES; GIVE THE PLANCK CONSTRAINT; SAY WHAT'S NEEDED TO MAKE PROGRESS) which is measured on the largest angular scales, a unique strength of a satellite like PICO.

In addition, the larger sky coverage improves the statistics of both the primary spectra and the lensing maps. This information can be combined to give new insights into the nature of dark matter and potential interactions with the Standard Model. (THE LAST TWO SENTENCES SEEM TO BE ABOUT DM; SHOULD WE HAVE A DIFFERENT PARAGRAPH?)

Light particles thermalized in the early universe leave a universal contribution to N_{eff} that is sensitive to the freeze-out temperature and then spin of the particle. A mission like PICO holds the promise to reach back to times when the temperature of the universe was orders of magnitude hotter than we have probe today. Such a measurement would shed light on the history of the universe at those very early times and can address important questions about the particles and forces in the Standard Model and Beyond.

Measuring CMB polarization at small angular scales will bring many of the questions about the universe into sharp focus. Of particular interest is the projected improvements to the number of relativistic species, N_{eff} . Light particles thermalized in the early universe leave a universal

contribution to N_{eff} that is sensitive to the freeze-out temperature and then spin of the particle. A mission like PICO holds the promise to reach back to times when the temperature of the universe was orders of magnitude hotter than we have probe today. Such a measurement would shed light on the history of the universe at those very early times and can address important questions about the particles and forces in the Standard Model and Beyond.

The CMB also offers a unique window into the *thermal* history of the universe, from the time of reheating through today. It is during these eras that the matter and radiation that fill the universe were produced and evolved to form the structures observed at low-redshifts. Measurements of the CMB on small angular scales are sensitive to the many components that make up the universe including the baryons, cosmic neutrinos, dark matter, and a wide variety of particles motivated by extensions of the Standard Model. The history of the universe prior to a few seconds is still largely unexplored observationally and potentially hides important clues to the nature of the fundamental laws and our cosmic origins.

CMB secondary anisotropies provides information into the growth and evolution of structure in our universe. CMB lensing, the thermal and kinetic Sunyaev-Zeldovich effects (SZ), and extragalactic point sources all contribute significantly to the CMB intensity fluctuations on small angular scales. The projected mass map from CMB lensing correlated with tracers of large-scale structure tomographically probes the how stucture grows. The thermal SZ provides a map of the integrated free electron pressure along the line of sight, and the peaks of this map trace all the galaxy clusters in the universe. In addition to τ , The epoch of reionizaton inprints information in the statistical moments of the kinetic SZ signal. Extragalactic point sources are becons for active galactic nuclei (in the radio) and dust emission from vigorously star-forming galaxies around redshift two and ealier.

2.2 Science Objectives (17.5 pgs)

The PICO Science Traceability Matrix (2pg, Hanany&Trangsrud) will be inserted around here. It is an 11x17 foldout, so it counts as 2 pages, which leaves 15.5 to all the rest in 2.2. Currently allocating 15 pages.

2.2.1 Fundamental Physics (6 pgs, Flauger, Green)

To include: Cosmic Inflation, Particle Physics (Neutrinos and Light Relics), primordial EM fields
Gravitational waves and inflation

Measurements of the CMB together with Einstein's theory of general relativity imply that the observed density perturbations must have been created long before the CMB was released, and rather remarkably even before the universe became filled with a hot and dense plasma of fundamental particles. What generated these perturbations is one of the biggest questions in cosmology.

While the dynamics of the plasma produces some amount of gravitational waves, the amplitude is too small to be detected in existing or planned CMB experiments. So any imprint of gravitational waves on the cosmic microwave background detected by PICO would constitute evidence for gravitational waves from the same primordial period that created the density perturbations. Because the dynamics of gravitational waves is essentially unaffected by the plasma physics, they would be a pristine relic left over from the earliest moments of our universe, and their properties would shed light on the mechanism that created the primordial perturbations that grew into the anisotropies of

the CMB and the stars and galaxies around us. Knowledge of the strength of the signal and their statistical properties would transform our understanding of many areas of fundamental physics.

Inflation, a period of nearly exponential expansion of the early universe, is the leading paradigm explaining the origin of the primordial density perturbations. It predicts a nearly scale invariant spectrum of primordial gravitational waves originating from quantum fluctuations. Thus, a detection of these gravitational waves would be the first detection of phenomenon associated with quantum gravity. Because the spectrum is scale-invariant, one may hope to detect primordial gravitational waves over a wide range of frequencies including, for example, at LIGO or LISA frequencies. However, as a consequence of the expansion of the universe, the energy density in the gravitational waves rapidly dilutes with increasing frequency, and observations of the CMB provide the easiest, and for the foreseeable future only way to detect these gravitational waves.

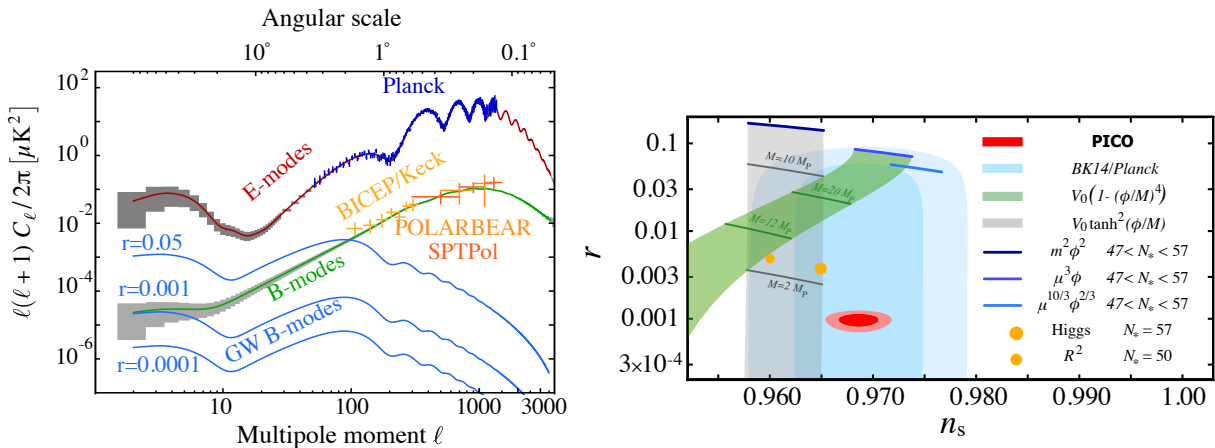


Figure 1: power spectrum place holder

The strength of the signal, often quantified by the tensor-to-scalar ratio r , is a direct measure of the expansion rate of the universe during inflation. Together with the Friedmann equation, this reveals one of the most important characteristics of inflation, its energy scale. PICO will be able to detect primordial gravitational waves if inflation occurred at an energy scale of at least 4×10^{15} GeV. A detection would have profound implications for fundamental physics because it would provide evidence for a new energy scale, and would allow us to probe physics at energies far beyond the reach of terrestrial colliders.

The signal would have two contributions, one on degree angular scales or multipoles of $\ell \sim 80$, typically referred to as the recombination peak, and another contribution for multipoles of $\ell \lesssim 20$ from reionization. The contribution from reionization is expected to be strongest relative to the contribution from weak lensing and instrumental noise. No sub-orbital experiment has meaningfully measured modes at $\ell < 40$ and a satellite like PICO is the most suitable approach to reach the lowest multipoles.

There are two classes of slow-roll inflation that naturally explain the observed value of the spectral index of primordial fluctuations, n_s . The first class is characterized by potentials of the form $V(\phi) \propto \phi^p$. This class includes many of the simplest models of inflation, some of which have already been strongly disfavored by existing observations. If the constraints on the spectral index tighten by about a factor 2 with the central value unchanged, and the upper limits on r improve by an order of magnitude, this class would be ruled out.

The second class is characterized by potentials that exponentially approach a plateau and in-

clude R^2 inflation. This model predicts a tensor-to-scalar ratio of $r \sim 0.003$. All models in this class with a characteristic scale in the potential that is larger than the Planck scale predict a tensor-to-scalar ratio of $r \gtrsim 0.001$, and an experiment like CMB-S4 could exclude these scenarios. However, there are models such as the Goncharov-Linde model with a somewhat smaller characteristic scale that predict a tensor-to-scalar ratio of $r \sim 4 \times 10^{-4}$.

In the absence of a detection, PICO would limit the amount of gravitational waves to $r < 10^{-4}$ at 95% CL. This is stronger than current upper limits by three orders of magnitude, and stronger than those expected for the ground-based experiment CMB-S4 by an order of magnitude.

Models of inflation, or the early universe more generally, differ in their predictions for the scalar spectral index n_s and its scale dependence, often referred to as the running of the spectral index n_{run} . With its high resolution and low noise levels, PICO will improve the constraints on n_s and n_{run} by a factor of about two. In addition, PICO will probe the statistical properties of the primordial fluctuations over a wide range of scales with exquisite precision and improve constraints on departures from Gaussianity by a factor 2 – 3.

Light relics

In the inflationary paradigm, the universe was reheated to temperatures of at least 10 MeV and perhaps as high as 10^{12} GeV. At these high temperatures, even very weakly interacting or very massive particles, such as those arising in extensions of the standard model of particle physics, can be produced in large abundances [1, 2]. As the universe expands and cools, the particles fall out of equilibrium, leaving observable signatures in the CMB power spectra. Through these effects the CMB is a sensitive probe of neutrino and of other particles’ properties.

One particularly compelling target is the effective number of light relic particle species N_{eff} , also called the effective number of neutrinos. The canonical value with three neutrino families is $N_{\text{eff}} = 3.046$. Additional light particles contribute a change to N_{eff} of $\Delta N_{\text{eff}} \geq 0.027 g$ where $g \geq 1$ is the number of degrees of freedom of the new particle [3, 4]. This correction to N_{eff} is a universal function of the decoupling temperature, with the range $0.07 g \geq \Delta N_{\text{eff}} \geq 0.027 g$ corresponding to decoupling from the just before the QCD phase transition back to reheating. A measurement of $\sigma(N_{\text{eff}}) \sim 0.03$ would reach orders of magnitude higher decoupling temperatures and extend our knowledge of extensions of the Standard Model, especially for particles with spin ($g \geq 7/4$).

Forecasts for N_{eff} are shown in Figure 2. The two most important parameters for improving constraints are the fraction of sky observed f_{sky} and the noise. Achieving both larger f_{sky} and lower noise are strengths of PICO compared to other platforms. Our baseline mission nearly reaches the target constraint with $g = 1$. A newly designed mission with only 10 times higher sensitivity will reach $\sigma(N_{\text{eff}}) < 0.025$. A high precision measurement of the CMB in temperature and polarization is the only proven approach to reach this important threshold.

Many light relics of the early universe are not stable. They decay, leaving faint evidence of their past existence on other tracers. The relics with sufficiently long lifetime to survive few minutes, past the epoch of light element synthesis, leave a signature on the helium fraction Y_p . If they decay by the time of recombination, their existence through this period is best measured through the ratio of N_{eff} to Y_p . PICO’s cosmic variance limited determination of the E mode power spectra will improve current limits for these quantities by a factor of five thus eliminating sub-MeV mass thermal relics.

Cosmological measurements have already confirmed the existence of one relic that lies beyond

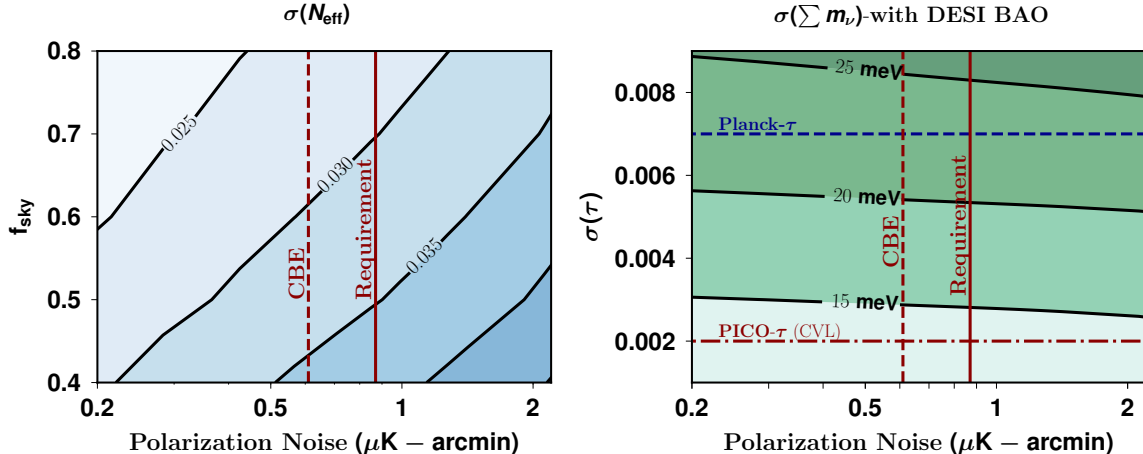


Figure 2: N_{eff} uncertainty as a function of noise and sky fraction (left) and sum of neutrino masses uncertainty as a function of noise and the uncertainty in the measurement of τ , for 0.7 sky fraction (right). The resolution assumed is $5'$. Vertical lines denote the expected performance of the baseline mission. The upper blue dashed line is the current *Planck* limit; the lower grey dashed line is the limit from cosmic variance limited measurement of τ . All forecasts assume internal delensing of the T and E -maps [5], including residual non-Gaussian covariances. The $\sum m_\nu$ forecasts include DESI BAO.

the Standard Model: dark matter. For a conventional WIMP candidate, the CMB places very stringent constraints on its properties through the signature of its annihilation on the T and E spectra [? ? ?]. *Planck* currently excludes WIMPs with mass $m_{\text{dm}} < 16$ GeV and a future CMB mission could reach $m_{\text{dm}} < 45$ GeV for $f_{\text{sky}} = 0.8$. The CMB provides the most stringent constraints on the dark matter annihilation cross section for dark matter in this mass range.

A particle-independent approach is to constrain dark matter interactions that would affect the evolution of the effective dark matter fluid and its interactions with baryons or photons. The simplest example is to constrain the baryon-dark matter cross section through its effective coupling of the two fluids [6]. These couplings affect the evolution of fluctuations and ultimately the T and E spectra. The current limits of $\sigma \lesssim 10^{-31} - 10^{-34} \text{ cm}^2 \times (m_{\text{dm}}/\text{MeV})$ can be competitive with direct detection for sub-GeV masses. More exotic dark sectors that include long-range forces can produce an even richer phenomenology in the CMB and in the large-scale structure without necessarily producing an associated signature in direct detection experiments or indirect searches (e.g. [7, 8, 9]).

Z

A host of other physical phenomena including the existence and properties of axions, primordial magnetic fields, and superconducting strings, leave signatures on the spectrum of the CMB and can therefore be constrained by the sensitive measurements of a future Probe [e.g., ? ? ? ? ?].

Neutrino mass

The origin and structure of the neutrino masses is one of the great outstanding questions about the nature of the Standard Model particles. Measurements of neutrinos in the lab have revealed much about the masses differences and mixing angles. Cosmology complements the ongoing effort in the lab by offering a measurement of the sum of the neutrino masses, $\sum m_\nu$, through the gravitational influence of the non-relativistic cosmic neutrinos (confirmed by the measurement of N_{eff}). The best current constraint arises from a combination of Planck and BOSS BAO to constraint $\sum m_\nu < 0.12$

eV (95%).

Cosmological measurements are primarily sensitive to the suppression of power on small scales after the neutrinos become non-relativistic, which can be measured via CMB lensing or weak lensing in a galaxy survey. However, these measurements are limited by our knowledge of the primordial amplitude, A_s . In practice, CMB observations most directly constrain $A_s e^{-2\tau}$ and thus do not provide a high precision measurement of A_s or τ .

Although many surveys hope to detect $\sum m_\nu$, any detection of the minimum value expected from particle physics $\sum m_\nu = 58$ meV at more than 2σ will require a better measurement of τ . The best constraints on τ come from E modes with $\ell < 20$ which require measurements over the largest angular scales. To date, the only proven method for such a measurement is from space. The current limit of $\sigma(\tau) = 0.009$ is from *Planck* [10]. Forecasts for a CMB measurement of $\sum m_\nu$ using the lensing B mode [11] are shown in Figure 2. With the current uncertainty in τ one is limited to $\sigma(\sum m_\nu) \gtrsim 25$ meV; no other survey or cosmological probe would improve this constraint. But PICO will reach the cosmic variance limit of $\tau \sim 0.002$ and will therefore reach $\sigma(\sum m_\nu) < 15$ meV when combined with DESI’s measurements of baryon acoustic oscillations [12]. Robustly detecting neutrino mass at $> 3\sigma$ in any cosmological setting is only possible with an improved measurement of τ like the one achievable with PICO.

Using a PICO measurement of τ to achieve $\sigma(\tau) < 15$ meV, implies that either PICO would capable of detecting $\sum m_\nu > 0$ at greater than 4σ or would exclude the inverted hierarchy ($\sum m_\nu > 100$ meV) at 95% confidence, depending on the central value of the measurement.

2.2.2 Cosmic Structure Formation and Evolution (4 pgs. Hill, Battaglia (& Alvarez))

Physics of Reionization

The reionization of the Universe imprints multiple signals in the CMB, in both temperature and polarization. In polarization, the most important reionization signal is the large-scale E -mode power sourced by the scattering of the temperature quadrupole during this epoch. This signal allows a direct measurement of the optical depth, τ_{au} , with very little degeneracy with other parameters (and, to some extent, a measurement of the reionization history itself). In contrast, inference of τ from the TT power spectrum is hindered by its direct degeneracy with the scalar fluctuation amplitude. Thus, large-scale EE power spectrum measurements are a unique and crucial observable to constrain this parameter. If measurements of τ are not improved beyond the current uncertainties from *Planck*, inference of several new aspects of cosmological physics (e.g., neutrino mass) will be severely hindered. PICO is the ideal experiment to make this measurement. Its noise level and frequency coverage permit a cosmic-variance-limited constraint on τ , i.e., $\sigma(\tau) \approx 0.002$. **Does this projected error bar need to be derived from the foreground simulations that are being used for r forecasting? Or is it obvious that if we can reach the $\sigma(r)$ target, this $\sigma(\tau)$ value can easily be achieved?**

In temperature, the most important small-scale imprint is that sourced by the “patchy” kinematic Sunyaev-Zel’dovich (kSZ) effect, due to the peculiar velocities of free electron bubbles around ionizing sources (e.g., galaxies or quasars). The total kSZ power spectrum receives contributions from both the patchy reionization signal and “late-time” sources, e.g., the intergalactic and intracluster media. The reionization and late-time signals are expected to have comparable amplitudes [? ? ?]. With constraints on the late-time contribution from other information (e.g., cross-correlations), effective small-scale foreground removal, and with the primary CMB TT power spectrum constrained by inference from the EE power spectrum, it is possible to extract reionization constraints

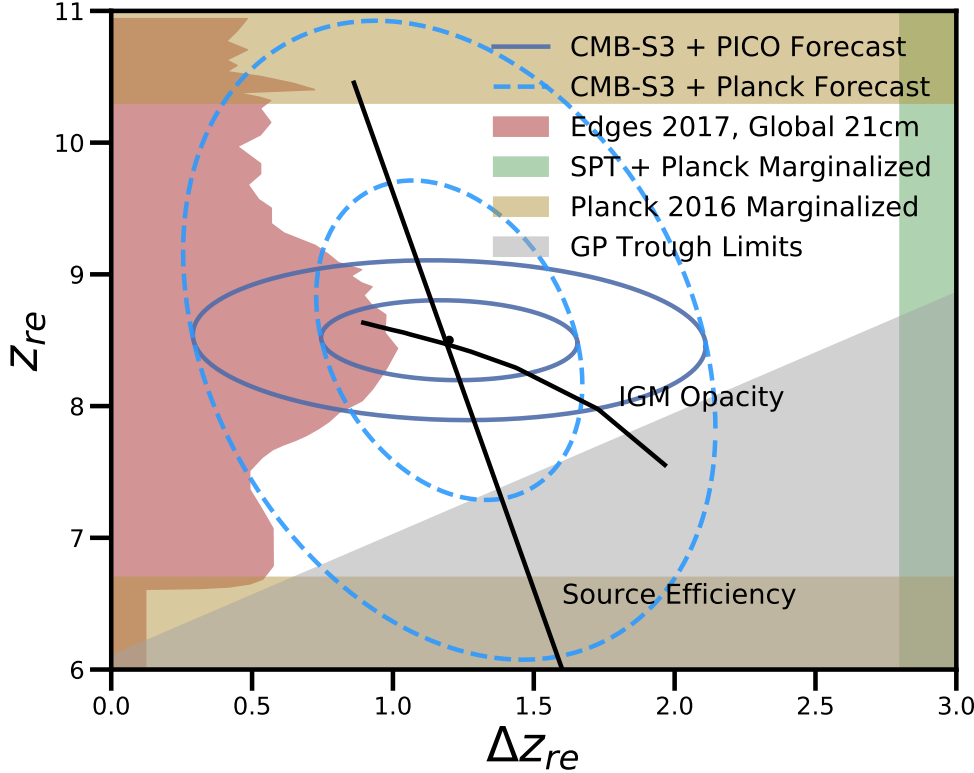


Figure 3: Summary of constraints on the mean redshift and duration of reionization. We reported forecasts show 68% and 95% confidence-level contours for PICO combined CMB-S3 experiments and Planck combined with CMB-S3 experiments (dark blue and dashed blue, respectively). The solid black lines illustrate how the IGM opacity and source efficiency model parameters map onto this parameter space. The PICO are compared to: The current exclusion limits for the mean redshift of reionization from Planck, shown by the yellow bands [?]; The recent exclusion limits from the global 21 cm signal measured by EDGES, shown with the red band [?]; The exclusion limits from measurements of the Gunn Peterson trough from fully absorbed Lyman alpha in quasar spectra, shown by the gray band [?]; And the exclusion limit on the duration of reionization from Planck and SPT data, shown by the green band [?].

from the small-scale kSZ power spectrum [?].

In addition to these signals, reionization also leaves specific non-Gaussian signatures in the CMB. In particular, patchy reionization induces non-trivial 4-point functions in both temperature [?] and polarization [?]. The temperature 4-point function can be used to separate reionization and late-time kSZ contributions. Combinations of temperature and polarization data can be used to build quadratic estimators for reconstruction of the patchy τ field, analogous to CMB lensing reconstruction. **Are we planning to try to forecast these here?**

FIGURE: τ constraint, kSZ power spectrum constraints, perhaps patchy τ reconstruction constraints? I assume the four-point estimator does not look promising given the relatively low resolution of PICO, but we can check the Smith papers. This will essentially be an analog of Fig. 39 of the SO forecasting paper (Nick and Marcelo have the relevant code).

The Sections below need to be rearranged to match other Science Objective(s) from the STM, but to also relay the breadth of science reachable by PICO, even if those goals are not in the STM.

Structure Formation via Gravitational Lensing

Measurements of the CMB reveal structure imprinted not only at the early time of recombination, but also at nearly every significant ensuing epoch in cosmic history. In particular the matter between us and the CMB last-scattering surface will deflect the path of CMB photons, a process known as gravitational lensing. Although the lensing of the CMB is a weak signal, targeted statistical estimators enable its extraction. The detection of the lensing signal has rapidly progressed, from the first detections in 2007-8 [13?] to the recent 40σ measurement by the *Planck* team [14]. When applied to a rich dataset such as that expected from the PICO satellite, these estimators will provide a map of all the matter in the Universe in projection, with the most sensitivity at redshift $z \simeq 2$ and down to scales of approximately ten arcminutes.

Forecasts show that the power spectrum of lensing in this map can be detected at approximately 580σ or 650σ for the requirement or CBE configurations, respectively. Such high signal to noise measurements represent an order of magnitude improvement over the current state of the art, obtained by the *Planck* team. Figure 4 shows noise curves from the reconstruction of CMB lensing.

Lensing breaks the highly symmetric configuration of primordial density fluctuations appearing as E modes on the sky, turning some of these into B modes. If not accounted for, this effect yields an noise floor on the large-scale B modes that can be measured from the early Universe. However, maps of E modes and of the lensing field, both of which will be obtained with PICO data, can be used together to create a template for these lensed B modes. This template can then be subtracted from the measured B modes to obtain improved performance, in a process known as “delensing” [15, 16]. Forecasts show that up to 80% of the lens-induced B mode power can be removed in the ‘requirement’ configuration, with this number becoming 85% for the current best estimate.

- Delensing and neutrino mass constraints assumed to go in fundamental physics chapter
- Cross-correlations: what to focus on here?
- CMB halo lensing: cluster mass calibration

Physics of Galaxy Formation via the Sunyaev-Zel’dovich (SZ) Effects

Not all CMB photons propagate through the universe freely, about 6% of them are Thomson-scattered by free electrons in the intergalactic medium (IGM) and intracluster medium (ICM). These scattering events leave a measurable imprint on CMB temperature fluctuations called secondary anisotropies, and they contain a wealth of information from how structure grows to the thermodynamic history of baryons. A fraction of these photons produce Sunyaev–Zel’dovich effects [? ?]. The thermal SZ effect (tSZ) is the increase in energy of CMB photons due to scattering off hot electrons. This results in a spectral distortion of the CMB blackbody that corresponds to a decrement in CMB temperature at frequencies below 217 GHz and an increment at frequencies above. The kSZ is the Doppler shift of CMB photons Thomson-scattering off free electrons that have a non-zero peculiar velocity with respect to the CMB rest frame. The amplitude of tSZ and kSZ proportional to the integrated electron pressure (tSZ) and momentum (kSZ) along the line of sight, thus contain information about the thermodynamic properties of the IGM and ICM. The tSZ effect can be used to ensemble statistics of galaxy clusters, which contain cosmological information as well as provide uniform cluster samples for galaxy formation studies in dense environments.

- Thermal SZ Effect
 - Cluster count forecast

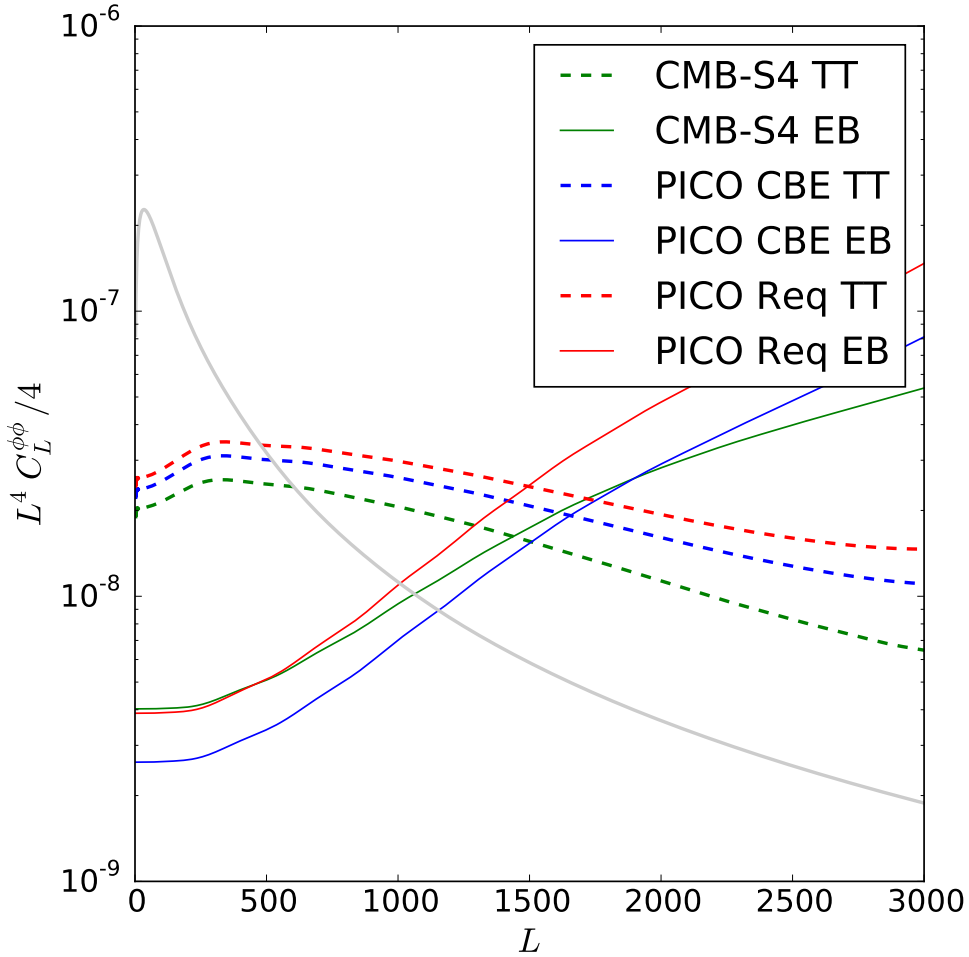


Figure 4: Lensing noise curves for various experimental configurations, showing the noise per mode of the reconstructed lensing field. The signal curve, the CMB lensing power spectrum is shown in grey; mapping of dark matter is possible at modes where the noise curves fall below this signal. Shown in solid are the performance of the *EB* polarization estimator, including iterated delensing; this estimator performs best on large angular scales. On smaller angular scales the temperature (*TT*) estimator shows the best performance. The associated signal to noise ratio for the lensing power spectrum is 570 for the 'requirement' configuration and 650 for the 'CBE' configuration.

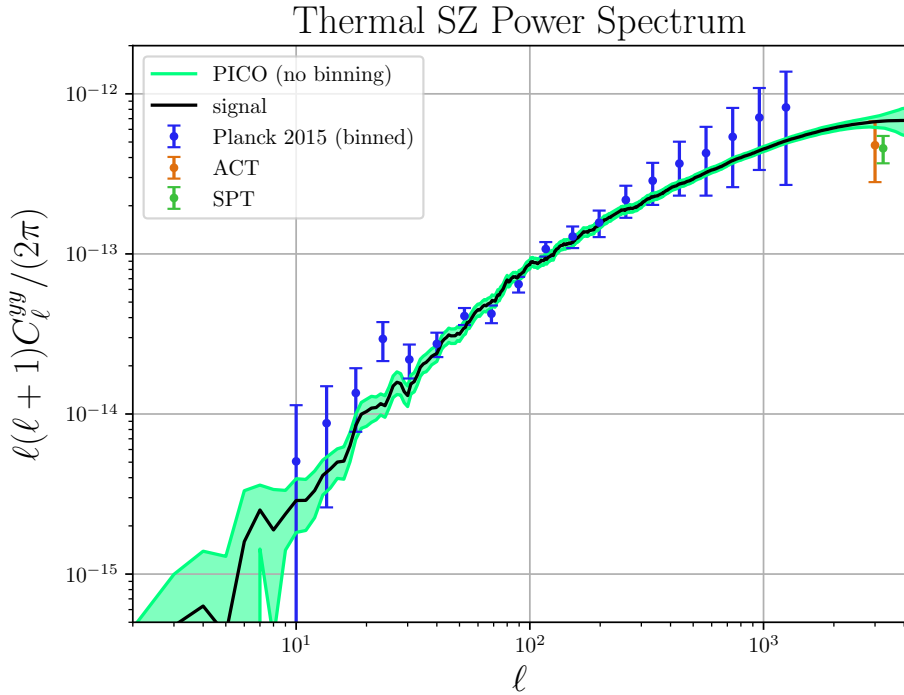


Figure 5: Constraints on the tSZ power spectrum from PICO and current data. The black curve shows the simulated tSZ power spectrum signal. The light green shaded region shows the error bars for PICO at each multipole, i.e., with no binning, as determined from NILC analysis of full-sky simulations. The blue points show the current constraints from Planck, which have been averaged into broad multipole bins. The orange and dark green points show the constraints from ACT and SPT, respectively, at a single multipole of $\ell = 3000$. The overall PICO $S/N = 1270$, nearly two orders of magnitude larger than current measurements.

- y -map and tSZ auto-power spectrum: figure with signal and NILC noise curve(s) [M. Remazeilles]
- Cross-correlations: forecast S/N with LSST, Euclid, DESI
- Kinematic SZ Effect
 - Cross-correlations: forecast S/N with LSST, Euclid, DESI
 - Constraints on ICM models: figure with gas pressure and density profile plots, error bars
 - Late-time kSZ power spectrum?

2.2.3 Galactic Structure and Star Formation (3 pgs, Chuss & Fissel)

Galactic Molecular Clouds

Stars form out of dense, gravitationally unstable subregions within molecular clouds. The efficiency of this conversion from molecular gas to stars is very low, as a result of the balance between turbulence, magnetic fields, feedback from young stars, and gravity over many scales in size and

density [?]. Magnetic fields may play an important role in slowing the star formation process, by inhibiting motions of gas in the direction perpendicular to the field. However the degree to which magnetic fields reduce star formation efficiency is poorly constrained because of the difficulty of making detailed maps of magnetic fields over a large sample of molecular clouds. With PICO we will answer the question of **how do the magnetic fields that thread clouds inhibit the formation of dense, gravitationally unstable sub-structures within molecular clouds, and how does magnetic regulation affect the efficiency with which stars form?**

PICO will measure dust polarization over the entire sky, and since dust grains are known to align perpendicular to their local magnetic field [? ?], these observations will be used to create detailed maps of magnetic field morphology. With a best $1.1'$ FWHM beam size PICO will be able to map all molecular clouds at better than 1 pc resolution out to 3.4 kpc . The BoloCam Galactic Plane Survey found 700 molecular clouds, recovering distances for approximately half their sample while covering roughly a third of the Galactic Plane [?]. PICO can therefore be expected to make highly detailed magnetic field maps of thousands of molecular clouds with thousands to hundreds of thousands of independent measurements per cloud, a huge improvement over the 10 nearby clouds mapped to the same level of detail with the *Planck* Satellite [?].

Our goal is to use the PICO observations to measure:

- *The Balance between Gravity and Magnetic Support.* This is parameterized by the mass-to-flux ratio $\mu = M/M_B$, comparing M , the mass of a gas cloud to $M_\Phi = \Phi/2\pi G^{1/2}$, the maximum mass that can be supported by the magnetic flux (Φ) through the cloud. Where $\mu > 1$ the cloud cannot be supported by the magnetic field alone. Current observations suggest that the envelopes of clouds can be supported against gravity by magnetic fields ($\mu < 1$), but higher density structures such as cores and filaments are supercritical ($\mu > 1$) and can thus collapse to form stars [?]. PICO will determine whether this model is true for all clouds and make detailed observations of the density scale magnetic flux is lost.
- *The Balance between Turbulence and Magnetic Fields.* Turbulence also plays a crucial role in star formation. The turbulent gas motions will determine the initial range of gas density within the molecular cloud. The balance between turbulent and magnetic fields, is characterized by the Alfvén Mach number $\mathcal{M}_A = \sigma_k/v_A$, where σ_k is the turbulent velocity width and $v_A = |B|/\sqrt{4\pi\rho}$ is the Alfvén velocity. If $\mathcal{M}_A < 1$ then the magnetic field is strong enough to significantly influence gas motions. Recent Planck observations of ten nearby clouds have shown that low column density cloud structures statistically tend to align parallel to the magnetic field [?], while high column density cloud structures have either no preferred alignment or in many cases align perpendicular to the magnetic field [?]. These observations can only be reproduced in simulations if the large-scale magnetic field within molecular clouds is as strong or stronger than turbulence [? ? ?]. PICO will determine whether the “strong field” case is true for molecular clouds of different ages and masses, and will measure the scale at which the cloud transitions from magnetic to turbulence and/or gravity dominated.

To measure these quantities we will apply established polarization analysis techniques:

- *Magnetic Field Dispersion:* Both [?] and [?] showed that in the interstellar medium the dispersion in magnetic field direction angles can be used to estimate the magnetic field strength, if the turbulent velocity dispersion is known. With PICO we will use the modern

variations of this method [? ? ?] by fitting a model polarization angle dispersion power spectrum in order to constrain the projected magnetic field strength ($|B_{POS}|$), turbulent to magnetic field ratio (\mathcal{M}_A), and magnetized turbulence power spectrum .

- *Polarization Modeling:* Measuring the statistical properties of the fraction of dust emission that is polarized and how this polarization level correlates with column density and magnetic field angle dispersion, can be used to constrain whether the field is strong or weak, where in the cloud is the magnetic field best traced, and how inclined the magnetic field is with respect to the plane of the sky [? ?].
- *Comparing Polarization and Velocity Gradients:* Gradients in spectral line velocity for atomic and molecular gas have recently been shown to align perpendicular to the magnetic field [? ? ?]. These gradients change from perpendicular to parallel to the magnetic field where the cloud becomes self-gravitating. Most PICO target clouds have already been observed with Galactic plane molecular line surveys such as CHAMP, ThRUmm, MALT-90, and SEDGISM, so by comparing PICO maps the velocity structure we can determine where the energy balance between gravity and magnetic fields change.
- *Cloud Structure Alignment the Magnetic Field:* Planck and BLASTPol observations have shown a statistically significant change in relative alignment of low (parallel) to high density (perpendicular) gas with respect to the magnetic field [? ? ?]. As discussed above, this is consistent with cloud formation simulations where $\mathcal{M}_A \leq 1$, or where the magnetic field is equal or stronger than the turbulent gas motions. The column density where the transition occurs seems to depend on both the degree of magnetization (\mathcal{M}_A), and formation history of the cloud [? ?].

Each of the above analysis methods has different uncertainties and limitations. However, by applying all four techniques to both PICO observations and synthetic polarization maps made from “observing” simulations of molecular clouds in models we will quantitatively compare theory and observations, strongly constraining both the magnetic field strength, Alfvén Mach number, mass-to-flux ratio. Once the magnetization parameters are determined by PICO, we can then compare the magnetization to the efficiency of star formation, measured from near and far-IR observations of protostars with *Herschel*, *Spitzer*, and *JWST*.

PICO’s ability to map thousands of clouds, is not possible with any other current or proposed polarimeter. This large sample size is crucial, because dust polarization observations are sensitive to only the magnetic field projected on the plane of the sky. Polarization maps, and therefore inferred magnetic field morphology will look very different for clouds of with different viewing angles, and also for young clouds versus clouds that have already formed stars that may provide radiative feedback. **Observing a large sample size of clouds will allow PICO to study the role of magnetic fields in star formation as a function age, mass, while accounting for statistically for different viewing angles.**

Dust Physics - Grain Alignment

The association of interstellar polarization with elongated dust grains aligned by the interstellar magnetic field is well established [? ? ? ?]. For a review see [?]. Without a quantitative theory of grain alignment, it is impossible to properly model the magnetic field in the ISM using interstellar polarization observations. The last decade has been marked by significant advancements in

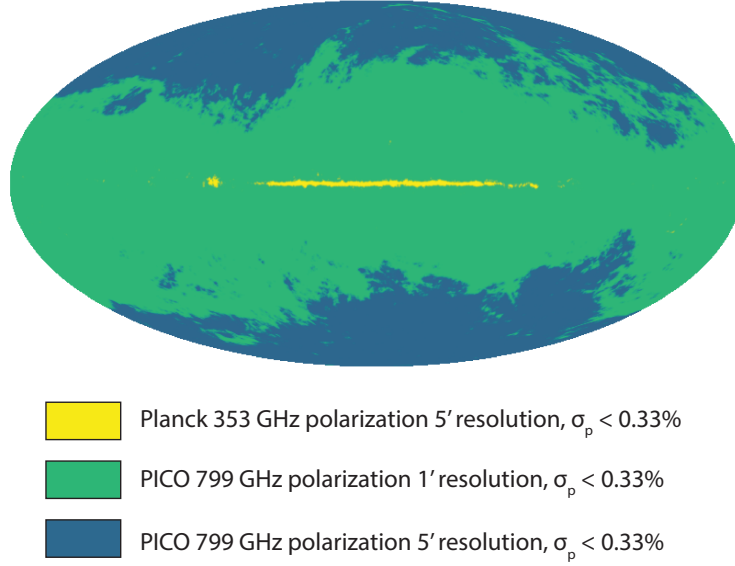


Figure 6: Caption

developing the quantitative theory of grain alignment. In particular, the analytical model of grain alignment by radiative torques [?] has been developed with some of its predictions successfully confirmed [? ?]. However, a number of key questions remain unanswered and this hinders the further progress of quantitative interpretation of the rich polarimetric data in relation to magnetic fields in the ISM.

In particular, the efficiency of radiative torque alignment depends on whether the grains have enhanced magnetic susceptibility [? ?] and whether the grain randomization is enhanced by magnetic turbulence [?]. Observational testing of the theoretical predictions, in particular, at the extremes of low and high density lines of sight, can finally provide the community with comprehensive theory of grain alignment. PICO with its high sensitivity and resolution is ideally suited to make these key observations.

Very low density lines of sight through dust near very luminous stars can be used to explore the transition in RAT from alignment with respect to the radiation, to alignment with respect to the magnetic field. This transition depends strongly on the grain magnetic susceptibility. PICO can explore grain alignment near hot stars with a strong UV continuum as well as cool stars, such as red giants and supergiants with much redder continua. These lines of sight will be very difficult to observe from balloon or airborne FIR and sub-mm polarimeters due to the low surface brightness and lack of all sky coverage.

At the other extreme, very high density lines of sight contain dust that is shielded from the interstellar radiation field, and show evidence for loss of grain alignment [?](Jones et al. 2015). PICO will not be able to fully spatially resolve all of these dense, molecular cloud cores, but it will be able to measure fractional polarization and column depth for thousands of cores. The many contributing factors influencing measurements of grain alignment in dense cores, such as the local field direction (as determined by the surrounding position angles), level of turbulence (as seen in the surrounding polarimetry), direction and proximity to luminous infrared sources, presence of an embedded YSO (which may provide Mid-Infrared flux to align grains), and the type of embedded YSO (luminosity and SED) can be separated statistically with this large sample, an impossible

task for ground based observations. These observations will provide a comprehensive assessment of grain alignment in dense molecular clouds. What measurements are necessary for this? Do we compare directions of polarization with magnetic fields measured in other ways? with radiation field directions? Are there critical complementary observations that we will assume/know we will have?

Dust Physics - Composition

Spectroscopic features observed in both dust extinction and emission reveal the materials that compose interstellar dust. Strong extinction features at 9.7 and 18 μm indicate much of the dust is in the form of amorphous silicates while features at 2175 Å, 3.3 μm , and 3.4 μm attest to abundant hydrocarbons. It is unknown, however, whether the silicate and carbonaceous materials coexist on the same grains (for instance, in a core-mantle structure) or whether they are segregated into distinct grain populations. If there are indeed multiple grain species, this will induce additional challenges for modeling the emission from interstellar dust in both total intensity and polarization at levels relevant for B-mode science [?].

Polarimetry allows clear discrimination between these scenarios. Spectropolarimetry of dust extinction features have yielded a robust polarization signal in the 9.7 μm silicate feature [e.g., ?], indicating that the silicate grains are aligned with the interstellar magnetic field. In contrast, searches for polarization in the 3.4 μm carbonaceous feature have yielded only upper limits, even along sightlines where silicate polarization is observed [? ?]. These data suggest that the silicate and carbonaceous materials cannot exist on the same grains. However, these studies are limited to only a few highly-extincted sightlines that may not typify the diffuse ISM.

Measuring polarized dust emission with PICO will provide a much more definitive test of these scenarios that extends to the most diffuse sightlines. If multiple dust species are contributing to the total dust emission, it is unlikely that they will all have identical SEDs, and therefore the fractional contribution of each grain type will vary with frequency. Likewise, it is unlikely that every grain type will have an identical intrinsic polarization fraction, and thus the total dust polarization fraction will vary with frequency. In contrast, the polarization fraction from compositionally homogeneous dust will be frequency-independent.

At odds with the spectropolarimetric evidence from dust extinction, current measurements of the polarization fraction of the dust emission with *Planck* [?] and BLASTPol [?] betray little to no frequency dependence across the full PICO frequency range (see Figure). While some models with multiple dust species are ruled out by these data, many models still fall within the current uncertainties. In addition, the current data at $\nu > 353 \text{ GHz}$ are from sightlines with much higher densities than the diffuse ISM, and thus may not be representative.

In addition to silicon and carbon, dust grains are a reservoir for most of the interstellar iron, some of which may be in the form of superparamagnetic inclusions [?]. The enhanced magnetic susceptibility from such inclusions results in the alignment from radiative torques becoming independent of the angle between the magnetic field and the radiation anisotropy [? ?], unlike for ordinary paramagnetic grains for which there is an explicit predicted dependence [?]. Thus, measuring grain alignment in the vicinity of bright stars with PICO, where the radiation direction is well-known, will provide a robust test for the presence of magnetic inclusions. Additionally, the emission from these inclusions will be polarized orthogonally to the electric dipole emission from the grain, leading to a decline in the polarization angle at low frequencies ($\nu \lesssim 100 \text{ GHz}$) and possibly a reversal in the polarization direction [?]. Thus, PICO will also place direct constraints

on the presence of magnetic inclusions through measurements of the dust polarization fraction.

In summary, PICO will dramatically improve the constraints on the properties of polarized dust emission and provide a definitive test of multi-component grain models, including the presence of magnetic inclusions. These insights will be directly inform modeling efforts in component separation

Meisner and Finkbeiner (2015) have determined a revised 2-component model for the diffuse Galactic thermal dust emission in the far-infrared.

$$I_\nu \propto 8570 \left(\frac{\nu}{GHz} \right)^{1.63} B_\nu(9.75K) + 1.49 \left(\frac{\nu}{GHz} \right)^{2.82} B_\nu(15.7K) \quad (1)$$

Assuming an independent polarization for each of the components, a simple model for the polarization can be articulated.

$$p = \frac{p_1 \times 8570 \left(\frac{\nu}{GHz} \right)^{1.63} B_\nu(9.75K) + p_2 \times 1.49 \left(\frac{\nu}{GHz} \right)^{2.82} B_\nu(15.7K)}{8570 \left(\frac{\nu}{GHz} \right)^{1.63} B_\nu(9.75K) + 1.49 \left(\frac{\nu}{GHz} \right)^{2.82} B_\nu(15.7K)} \quad (2)$$

Applying the noise estimates from PICO, 1000 simulations were run for each combination of polarization values for the two temperature components. Only frequency channels 107 GHz and above are used, and the simulated data are binned to the 7.9 arcminute beam of PICO’s 107 GHz channel. The uncertainties in each of the resulting polarization fractions were estimated from the variance of the simulation results. The resulting uncertainty of the warmer component is expected to be 1.7% and that of the colder component is expected to be 1.3%.

Diffuse Interstellar Medium

The diffuse ISM fills most of the volume of the Milky Way. It is a multi-phase medium, with magnetic fields, cosmic rays, and turbulence in rough energy equipartition [e.g., ?]. As the material that condenses to form molecular clouds, and eventually stars, and the material into which supernovae explode, the diffuse ISM is sculpted by a range of physics over many scales. Despite its importance, a comprehensive understanding of the diffuse ISM is challenging because of its diverse composition, its sheer expanse, and the multi-scale nature of the physics that shapes it. PICO is poised to revolutionize this field. With the unprecedented dynamic range summarized in Figure 6, PICO will drastically expand our ability to study the diffuse ISM both as a function of environment and as a function of physical scale. Here we detail a few of the scientific areas where PICO will answer major open questions.

Diffuse Interstellar Medium - Structure Formation

Recent high-resolution observations of the diffuse ISM have revealed a wealth of complex structure, deeply influenced by the structure of the ambient magnetic field. The structure of the cold neutral medium (CNM) in particular is highly anisotropic, largely organized into filamentary structures that are aligned with the magnetic field [?]. Alignment between linear ISM structures and the magnetic field traced by dust polarization has recently been measured in both neutral hydrogen [? ?] and dust emission [?]. The statistical properties of the density-magnetic field correlations can be described by cross-correlating the dust temperature (T) with the dust polarization field, decomposed into the rotationally invariant E - and B -modes. These measurements were made for the first time with *Planck*, with several unexpected results. There is a positive TE correlation in the

diffuse ISM, as well as a nonunity ratio of E -mode to B -mode polarization ($EE/BB \sim 2$). These correlations are currently thought to be caused by the preferential elongation of density structures along the magnetic field [? ?]. How do these quantities depend on scale and Galactic environment? The sensitivity and dynamic range of PICO will enable us to answer this question, which may in turn constrain properties of interstellar turbulence [e.g., ? ?].

Perhaps even more surprisingly, the final *Planck* data release reported a nonzero TB correlation across a range of scales in the diffuse ISM [?]. Such a correlation implies that the density-polarization correlation is not parity invariant. PICO will make a much higher-fidelity measurement of the TB correlation, and will either confirm or refute the *Planck* detection. PICO will also constrain the EB correlation value across the sky: EB was found to be zero within *Planck* uncertainty, but positive TE and TB correlations imply that at least a weak EB correlation should exist. The origin of the TB correlation is unknown. It has been speculated that the TB correlation could be due to nonzero magnetic helicity, or some other parity-violating MHD property, or that the low-multipole TB correlation may be related to the structure of the local large-scale magnetic field. PICO will test parity violation in the diffuse ISM, constrain models of magnetic helicity, and test models of the local Galactic magnetic field. **Is this an opportunity for a figure showing how much better PICO will do for power spectra? Or maybe the cosmology sections have this covered**

Structure formation in the diffuse ISM is a key area of study motivating observations across the electromagnetic spectrum. PICO’s observations will complement recently completed high dynamic range neutral hydrogen (HI) surveys, such as HI4PI [?] and GALFA-HI [?], as well as planned surveys of interstellar gas, most prominently with the Square Kilometer Array (SKA) and its pathfinders. One of the open questions in diffuse structure formation is how gas flows within and between phases of the ISM. A planned all-sky absorption line survey with SKA-1 will increase the number of measurements of the ISM gas temperature by several orders of magnitude [?]. Quantitative comparisons of the ISM temperature distribution from SKA-1 and estimates of the magnetic field strength and coherence length scale from PICO will elucidate the role of the magnetic field in ISM phase transitions.

2.3 Legacy Surveys (2 pgs, de Zotti)

Describe science that we get for free.

2.3.1 Point extragalactic sources in the PICO frequency range

As illustrated by the left panel of Fig. 7, at $\lambda \gtrsim$ few mm the dominant extragalactic population are blazars (flat-spectrum radio quasars, FSRQs, and BL Lacs), typically at $z \gtrsim 1$; the solid blue line shows an example. At shorter wavelengths dusty galaxies take over. The brightest sources in this spectral range are nearby star-forming galaxies like M 61. PICO will also see the brightest high- z sub-mm sources which, due to the “magnification bias”, are those whose flux density is boosted by strong gravitational lensing.

Herschel surveys have shown that, at 500 μm (600 GHz), about 20% of galaxies at the PICO detection limit are strongly lensed (right panel of Fig. 7). This is an extraordinary selection efficiency: for comparison, the fraction of strongly lensed galaxies is of $\sim 10^{-3}$ in all other frequency bands where searches have been carried out. Also, these galaxies have sub-mm colors substantially different from those of the other extragalactic populations and are therefore very easily singled out [18].

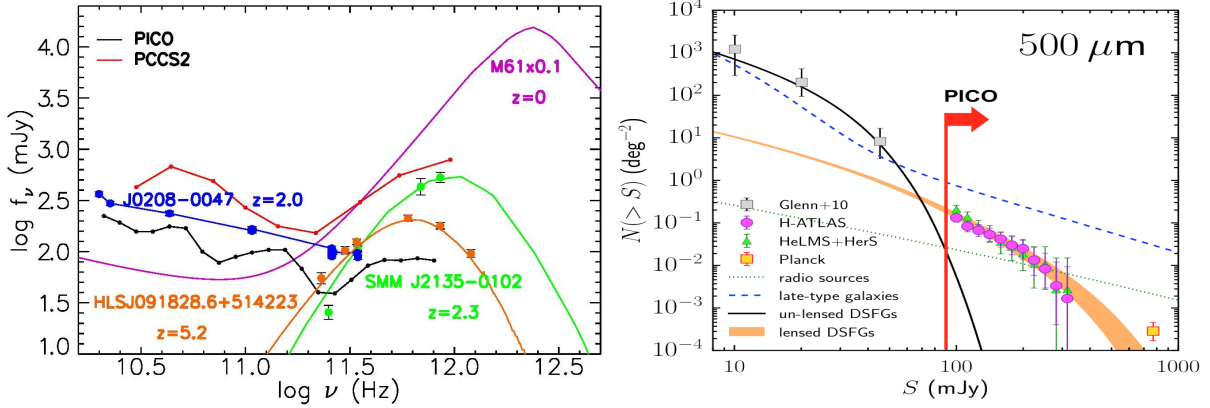


Figure 7: Left panel. Examples of SEDs of extragalactic sources detectable by PICO, compared with its point source detection limits (solid black line). The SED of M 61 has been scaled down by a factor of 10. The 90% completeness limits of the Second *Planck* Catalogue of Compact Sources (PCCS2; [17]) are also shown. **Right panel.** Integral counts of the various populations of extragalactic sources at $500 \mu\text{m}$ as determined by *Herschel* surveys. The vertical red line shows the estimated PICO detection limit.

PICO will detect several thousands strongly lensed galaxies. Objects like the $z = 4$ source HLSJ091828.6 + 514223 (left panel of Fig. 7; [19]) would be detectable by PICO up to extreme redshifts ($z > 10$).

The availability of thousands of strongly lensed galaxies opens exciting prospects both on the astrophysical and on the cosmological side (cf., e.g., ref. [20]). Compared to searches in other wavebands, PICO detections will extend to much higher redshift sources [most optically-selected strongly lensed galaxies are at $z < 1$, cf. Fig. 7 of ref. 20] and will pick up the rare most extreme amplifications, thanks to its all sky coverage: the magnification factors, μ , of “*Planck* dusty GEMS” are estimated to be of up to 50 [21].

Sub-mm lensing allows us to probe the most active star-formation phases, hardly visible in the optical. The gravitational flux boosting is accompanied by a stretching of images. Thus follow-up with ALMA can achieve an effective resolution of several milli-arcsec, i.e. can measure galactic structures at $z \simeq 3$ down to the astounding level of $\sim 50 - 60$ pc, much smaller than the sizes of Galactic giant molecular clouds [22]. This provides unique direct information on the mechanisms driving the star-formation and on the shapes, sizes and surface brightnesses of star-formation regions.

The detection of several thousands of galaxies at redshifts $\gtrsim 1$ and up to $z > 5$ allows a substantial progress towards a complete census of the dust-enshrouded star-formation history of the universe, i.e. towards tracking the buildup of stellar mass over cosmic time, in particular over epochs of most intense star formation.

The high redshifts of magnified galaxies imply high redshifts of foreground lenses. Optical follow-up will allow us to investigate the total (visible and dark) mass of the lensing galaxies, their density profiles, dark matter sub-structures in a much higher redshift range than in the case of optical selection [23].

Also PICO will explore essentially the entire Hubble volume for the most intense hyperluminous starbursts, testing whether there are physical limits to the star-formation rates of galaxies.

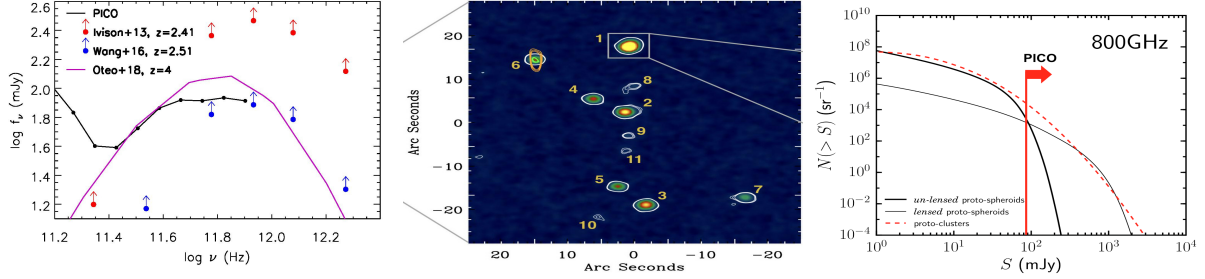


Figure 8: **Left panel.** SEDs of the cores of two proto-clusters of starbursting galaxies discovered by [26] at $z = 2.41$, by [27] at $z = 2.506$ and by [28] at $z = 4.0$. The first two SEDs include only the contributions of proto-cluster members within $10''$, i.e. over an angular size below the PICO resolution, corresponding to physical radii $\simeq 80$ kpc, substantially smaller than the effective proto-cluster sizes. The reported flux densities are therefore lower limits to those that will be measured by PICO. The SED of the $z = 4.0$ proto-cluster correspond to a SFR of $6500 M_{\odot} \text{ yr}^{-1}$, estimated by [28] summing the contributions of galaxies detected by ALMA within a radius of $\simeq 25''$; again this is likely a lower limit to what PICO will measure. The solid black line shows the PICO detection limits. **Central panel.** ALMA image of the $z = 4.0$ proto-cluster discovered by [28], extracted from Fig. 1 of their paper. **Left panel.** Counts of proto-clusters at 800 GHz predicted by the model of ref. [29]. The vertical red line corresponds to the PICO detection limit.

The right panel of Fig. 7 also shows that PICO will detect tens of thousands star forming galaxies in the nearby universe, reaching a surface density about a factor of two higher than that of the IRAS satellite at its $60 \mu\text{m}$ completeness limit [24]. The IRAS wavebands are relatively insensitive to low temperature dust emission, a significant and largely unexplored component of many nearby galaxies [25]. PICO will provide a full characterization of this component, complementing IRAS data to establish well calibrated dust SEDs as a function of galaxy morphology, luminosity, dust and gas mass, etc..

2.3.2 Early phases of cluster evolution

PICO will open a new window for the investigation of early phases of cluster evolution, when their member galaxies were actively star forming and before the hot IGM was in place. In this phase traditional approaches to cluster detection (X-ray and SZ surveys, searches for galaxy red sequences) work only for the minority of evolved objects; indeed they have yielded only a handful of confirmed proto-clusters at $z \gtrsim 1.5$ [30]¹.

SEDS of spectroscopically confirmed sub-mm-bright proto-clusters detectable by PICO are shown in the left panel of Fig. 8). *Planck* has demonstrated the power of low-resolution surveys for the study of large-scale structure [31] but its resolution was too poor to detect individual proto-clusters [29]. As illustrated by the central panel of Fig. 8, the typical sizes of high- z proto-cluster cores are of $\sim 1'$ (cf. also ref. [32]), nicely matching the PICO FWHM at the highest frequencies.

CMB Probe will detect many tens of thousands of these objects (right-hand panel of Fig. 8) up to $z \gtrsim 4$ (left panel). This will allow a real breakthrough in the observational validation of the formation history of the most massive dark matter halos, traced by clusters, a crucial test of

¹More high- z proto-clusters have been found targeting the environment of tracers of very massive halos, such as radio-galaxies, QSOs, sub-mm galaxies. These searches are however obviously biased.

models for structure formation. Follow-up observations will characterize the properties of member galaxies, probing the galaxy evolution in dense environments and shedding light on the complex physical processes driving it.

2.3.3 Radio sources

PICO will increase by orders of magnitude the number of blazars selected at sub-mm wavelengths and will determine the SEDs of many hundreds of them up to 800 GHz. The most luminous high- z FSRQs were found to host black holes (BHs) with the largest masses, up to $\sim 4 \times 10^{10} M_{\odot}$ (S5 0014 + 813, at $z = 3.366$; see ref. [33]). Such objects have particularly hard mm-wave spectra; thus PICO surveys are well suited to detect them. Objects like S5 0014 + 813 are detectable by PICO up to $z > 5$.

Blazar searches are the most effective way to sample the most massive BHs at high z because of the Doppler boosting of their flux densities. Since the flux boosting occurs for jets closely aligned with the line of sight ($\theta < 1/\Gamma$, $\Gamma \sim 15$ being the bulk Lorentz factor), for each FSRQ there are other $2\Gamma^2$ (i.e. hundreds) sources of similar intrinsic properties but pointing elsewhere.

Very large BH masses at high- z challenge models because it is very hard to grow a seed BH from stellar mass to $> 10^9 M_{\odot}$ in the limited age of the universe. It is even more so for jetted quasars because jets are likely associated with rapidly spinning BHs whose radiative efficiency is large so that the mass growth is slow. Yet at least 4 FSRQs has been discovered at $z > 5$ (up to $z = 5.48$; [34]). One (SDSS J013127.34032100.1 at $z = 5.18$) has estimated BH mass of $\sim 10^{10} M_{\odot}$ [35].

The PICO surveys of the largely unexplored mm/sub-mm spectral region will also offer the possibility to discover new transient sources [36] or events, such as blazar outbursts.

2.3.4 Source polarization

PICO will make a giant leap forward in the determination of polarization properties of both radio sources and of dusty galaxies over a frequency range where ground based surveys are impractical or impossible. Thanks to its high sensitivity, it will detect in polarization both populations over a substantial flux density range, determining directly, for the first time, number counts in polarized flux density.

Mm/sub-mm polarimetry of radio sources provides unique information on the magnetic field configuration (geometry and degree of order) in the innermost, unresolved regions of the jets, close to the active nucleus. Polarimetry of dusty galaxies as a function of their inclination is informative on the structure and on the ordering of their large-scale magnetic fields.

2.4 Complementarity with Other Surveys and with Sub-Orbital Measurements (1 pg, Lawrence, Schmittfull)

Should describe complementarity with other astrophysics surveys (both space and ground) and with sub-orbital CMB measurements. For the astrophysical surveys, this is summary text of text that is presumably sprinkled elsewhere in the proposal; please cross-reference.

2.4.1 Complementarity with Astrophysical Surveys in the 2020s

For cosmological constraints on the sum of neutrino masses, there is no known way to achieve $\sigma(\sum m_\nu) < 25 \text{ meV}$ without improving measurements of the optical depth τ over *Planck*'s low- ℓ polarization constraint (see the neutrino mass section above). In particular, this applies to all methods that rely on comparing low-redshift structure with the amplitude of the CMB at high redshift, such as galaxy clustering, weak lensing, or cluster counts. (Should add a sentence on ongoing work that attempts to get around τ : still not possible to do better than 25meV even with LSST and CMB-S4.) Improving τ and therefore $\sigma(\sum m_\nu)$ is only possible by improved observations of low- ℓ E modes, which are only possible from space. With its improved τ measurement PICO would therefore directly improve neutrino mass constraints when combined with late-time probes, reaching $\sigma(\sum m_\nu) < 15 \text{ meV}$. PICO therefore complements all efforts that probe the late time structure of the Universe to constrain the sum of neutrino masses, and combining PICO with these low-redshift observations enables more than any cosmological experiment could achieve on its own.

Reconstructing the CMB lensing convergence on very large angular scales, $L_\kappa < 20$, requires exquisit systematics control over a large sky fraction as well as high angular resolution to perform the lensing reconstruction. A space mission like PICO would provide that, complementing ground-based CMB lensing reconstructions that typically observe smaller sky fraction (or at least have different observation noise in different areas of the sky due to scanning strategy), which makes it difficult to reconstruct lensing on the largest scales. Indeed, PICO could robustly measure the lensing signal with a power spectrum signal-to-noise ratio of more than 100 per mode on very large scales (based on Alex Van Engelen noise plot from PICO meeting; is this still up to date?). Such high-significance CMB lensing measurements on the very largest scales can be useful when combined with measurements of galaxy clustering to search for local primordial non-Gaussianity via its scale-dependent effect on galaxy bias. In an idealized forecast, we find $\sigma(f_{\text{NL}}) \simeq 0.5$ for $L_{\min}^{\kappa\kappa,\kappa g,gg} = 4$, and $\sigma(f_{\text{NL}}) \simeq 0.9$ for $L_{\min}^{\kappa\kappa,\kappa g,gg} = 20$, assuming optimistic LSST galaxy clustering with 60 arcmin^{-2} galaxies and with high-redshift dropout galaxies. This would be a notable improvement over the best current constraint $\sigma(f_{\text{NL}}) = 5$ from *Planck*. Such a measurement would ultimately likely be limited by limitations of LSST on the very largest scales, but space based observations of galaxy clustering with Euclid or SPHEREx could help in this regard.

2.4.2 Complementarity with Sub-Orbital Measurements

Since the first measurements that recognized the existence of the CMB were made in 1964, important observations have been made from the ground, from balloons, and from space. The question for the future is what should the roles be of these three types of experimental approaches? To answer this question, start by considering the advantages and disadvantages of each location (Table ?).

Characteristic	Ground	Balloon	Space
Performance			
Sky coverage	Partial from single site	Partial from single flight	Full. Scan strategy not limited by atmosphere or ground. Large fractions of the sky can be observed nearly simultaneously with the same detectors.
Frequency coverage	Limited to atmospheric “windows”, which get increasingly opaque at higher frequencies. The frequency range where astronomical foregrounds are minimum is inaccessible from the ground, and frequencies above 300 GHz are unusable.	Better than ground. Foreground-minimum frequencies still unusable.	Unrestricted
Angular resolution	Telescope cost a function of size, but arcminute resolution possible.	Restricted to small telescopes. Arcminute resolution effectively impossible.	Telescope cost a steep function of size. Arcminute resolution very expensive.
Backgrounds and noise	Hundreds of K loading of detectors from atmosphere and ground, plus direct noise. Individual detector sensitivity reduced substantially, with $250 \mu\text{K s}^{-1/2}$ the practical limit for a single direct detector.	Atmospheric loading much less than from ground, but still greater than from space.	Only CMB, CIB, and Galactic backgrounds. Individual direct-detector sensitivities roughly an order of magnitude better.
Integration time	Limited by Sun, weather.	Severely limited by flight time. To date, tens of days per flight.	Continuous observations for years.
Practicalities			
Accessibility, repairability	Good	None. Multiple flights sometimes possible.	
Mass	Not a big issue	Big issue	Big issue

In every respect affecting performance, space has the advantage, and there can be no argument that space will be required to reach the ultimate limits set by astronomical foregrounds. But the advantages of space come at a high cost, in both time and money, and an essential question is how much can be done from the ground and balloons first? The answer depends on the specific requirements of the science questions being addressed, which we discuss below. However, some general guidelines can be given. When the entire sky is needed, as for fluctuations on the largest angular scales, space is necessary. The difficulties of controlling systematic errors and foregrounds over the whole sky at a level significantly below what has been achieved by Planck are simply too great to overcome on the ground. Progress on the reionization bump ($2 \leq \ell \leq 12$), whether for τ or for r , requires space. Significant progress can surely be made from the ground on the

recombination bump ($30 \leq \ell \leq 300$), and the $r \approx 10^{-3}$ goal of the “ultimate” ground-based experiment CMB-S4 looks to be both bold and achievable. For r , the confusing signal from large-scale-structure lensing of CMB E -modes into B -modes must be measured and removed, and this requires observations on sub-degree scales over a wide frequency range (because of foregrounds) that especially at the lower frequencies is a challenge from space.

The PICO r goal of 10^{-4} is beyond the reach of ground observations. The limited frequency range observable from the ground is not enough to separate foregrounds to the necessary level, and at 10^{-4} there is no room to give up any advantage on systematics. For science requiring higher angular resolution, however, such as observations of galaxy clusters at 1 arcmin resolution, the ground has a clear advantage.

(need more in here)

Balloon observations have been valuable in the past, but the severe limitations on observing time must be recognized. Even the ultra-long-duration balloons that have been on the horizon for more than two decades but have not yet flown for any astrophysics experiment offer only 10^2 days per flight, 5–10% of the duration of the Planck mission (depending on instrument), and 3% of the duration of WMAP. Both WMAP and Planck showed the essential power of repeated observations in identical conditions in revealing and controlling systematics. This will never be possible with balloon experiments. Reaching 10^{-4} will require vigorous exploitation of *every* possible advantage. There is nevertheless still an important role for balloon experiments, in demonstrating new technologies, and in training of students.

2.5 Signal Separation (4 pgs, Jacques and Clem)

Let’s make clear that there are numerous signals that need to be separated; rather than a ‘signal’ and ‘foregrounds’. Contamination of CMB observations by astrophysical foreground emission of various origins is one of the major challenges that future observations of CMB polarization must face. Polarized emission in the PICO frequency range is known to be dominated by synchrotron emission from the galactic interstellar medium in our own galaxy and by thermal emission from interstellar dust. Although much has been learnt about these polarized foregrounds with WMAP and Planck observations, their exact properties are not known at the level that would be needed to guarantee that they can be separated out from the CMB using known component separation techniques. In particular neither the exact form one should assume for the frequency scaling of their emission (if any), nor the variation of these emission laws across the sky or along the line of sight, nor the small-scale distribution of emission, are known at the required level of detail. Whether other processes emit at a level that can contaminate PICO observations significantly is also not known at present.

The many frequency channels of PICO can be used to learn from the PICO observations themselves the properties of these foregrounds, and to identify the CMB contribution in the multifrequency data using its unique spectral signature. To be robust against our uncertainty about the foregrounds, we assess the feasibility of foreground cleaning for different models of foreground emission of varying complexity, from optimistic to pessimistic, and for various component separation methods.

To assess the performance of PICO we have carried out map based simulations within a “data challenge” framework. In this process one group prepares sets of simulated maps which are placed in a shared area. These are then re-analyzed by multiple individuals and groups employing various different component separation algorithms.

2.5.1 PICO Map Based Simulations

For the CMB we take realizations of lensed- λ CDM shared from the Planck FFP10 simulation set. For the noise we take white noise realizations with the appropriate levels at each of the 21 bands. For the foregrounds we use a suite of 3rd party models:

- **00:** Simple Gaussian realizations of synchrotron and dust with power-law angular power spectra at amplitudes set to match the observations in the BICEP/Keck field, and simple uniform SEDs (power law for synchrotron, greybody for dust).
- **01:** The PySM² model `a1d1f1s1`, where the letters refer to anomalous microwave emission, dust, free-free and synchrotron respectively, and the numbers are the base models described in [?].
- **02:** The PySM model `a2d4f1s3`, where the models have been updated to variants that are also described in [?]. Note that these include 2% polarized AME, a curvature of the synchrotron SED, and a two-temperature model for dust.
- **03:** The PySM model `a2d7f1s3`, where the dust model has been updated to a sophisticated physical model of dust grains as described in [?]. This model is interesting in that it does not necessarily conform to the greybody SED.
- **06:** A model based on MHD simulations [?] of the Galactic magnetic field, which naturally produces non-Gaussian correlated dust and synchrotron emission.
- **08:** A multilayer model of dust [?] which seeks to include the variation of the SED along the line of sight—i.e. in this model the behavior does not conform to a single greybody even within a high resolution pixel (as it will not in reality).
- **09:** A model of dust and synchrotron which implements non-Gaussian smaller scale structure and includes some decorrelation of the dust pattern as a function of frequency [?].

2.5.2 Needlet re-analyis

The NILC is based on Internal Linear Combinantion (or ILC in short) component separation method. It has been applied to the PICO simulations to determine the angular power spectrum of the B-mode polarized CMB signal. This method only attempts to reconstruct the CMB signal, without using any prior information about foregrounds. It is based on two specific assumptions. Firstly, that the CMB is frequency independent in thermodynamic unit, and secondly, that the CMB is uncorrelated with foreground signals. The ILC method then estimates the CMB, S_b , as a weighted linear combination of the set of input multi-frequency sky maps such that the variance of the estimate is minimum, with unit response to the flat CMB frequency spectrum,

$$\widehat{S} = w^T X = \frac{a^T \widehat{R}^{-1}}{a^T \widehat{R}^{-1} a} X = \frac{a^T \widehat{R}^{-1}}{a^T \widehat{R}^{-1} a} (aS + F + N), \quad (3)$$

where X is the vector of frequency maps, a the constant frequency spectrum of the CMB signal S , F the total foreground signal, N the instrumental noise for the different frequency channels, and

²https://github.com/bthorne93/PySM_public

R_b the frequency-frequency covariance matrix. The first condition guarantees minimum contamination by foregrounds and instrumental noise whereas the second condition guarantees that the CMB signal is conserved without bias. The presence of the foregrounds induces correlated errors across frequencies, so that the ILC weights adjust themselves to minimise the foreground residuals present in the weighted linear combination. However, in reality the weights result from a trade-off between minimising the foregrounds and minimising the instrumental noise contribution in the reconstructed CMB map.

The ILC method can be straightforwardly implemented in either real (pixel) space or in harmonic space. Thus, sets of ILC weights can either be computed for different regions of the sky or for different angular scales, respectively, which allows for variations of the data covariance matrix in either space. However, the ILC in harmonic space does not take into account the fact that noise can be a significant source of CMB measurement error in at high Galactic latitude, while foreground signals are more important at low Galactic latitude. Conversely, the ILC in pixel space does not take into account the fact that the noise dominates on small angular scales, while diffuse Galactic foreground emission dominates on large angular scales.

In order to overcome this problem, we implement the ILC on a frame of spherical wavelets called needlets, a component-separation approach that we now refer to as the Needlet Internal Linear Combination (NILC) method. This technique has already been applied broadly in CMB data analysis. The needlets enable localised filtering in both pixel space and harmonic space because they have compact support in the harmonic domain, while still being very well localised in the pixel domain. The needlet decomposition allows the ILC weights to vary both smoothly on large angular scales and rapidly on small angular scales, which is not possible by sub-dividing the sky into different areas prior to any processing.

To analyse the simulations of sky for PICO, we have used 11 frequency channels (i.e. every alternate channels starting from the lowest frequency channel) and 11 needlet filters for the analysis. The needlet filters, h_l^j , in harmonic space that we use in our analysis are defined as follows,

$$h_l^j = \begin{cases} \cos \left[\left(\frac{l_{peak}^j - l}{l_{peak}^j - l_{min}^j} \right) \frac{\pi}{2} \right] & \text{for } l_{min}^j \leq l < l_{peak}^j, \\ 1 & \text{for } l = l_{peak}, \\ \cos \left[\left(\frac{l - l_{peak}^j}{l_{max}^j - l_{peak}^j} \right) \frac{\pi}{2} \right] & \text{for } l_{peak}^j < l \leq l_{max}^j \end{cases} \quad (4)$$

The simulated sky maps are first convolved or de-convolved in harmonic space to put them all at the same angular resolution (FWHM 15 arcmin) prior to the application of the NILC algorithm. Since the method as currently implemented is applicable to scalar fields on the sphere, sky maps of the B modes are constructed from the input Stokes parameters, Q and U, on the full sky. The NILC weights used to combine the multi-frequency input data in order to estimate the CMB signal are then computed from the full-mission sky maps for B-mode. The derived weights are also applied to the half-mission maps, which are later used for minimising the impact of residuals of noise on the measurement of angular power spectrum.

The needlet weights are mostly determined by the galactic contamination, which dominates on large angular scales, and by the noise level, which dominates on small angular scales. Although the weights of for a subset of the frequency channels under consideration are relatively low compared to other channels, they are important for removing the Galactic foreground contamination.

Table 1: List of needlet bands used in the present analysis.

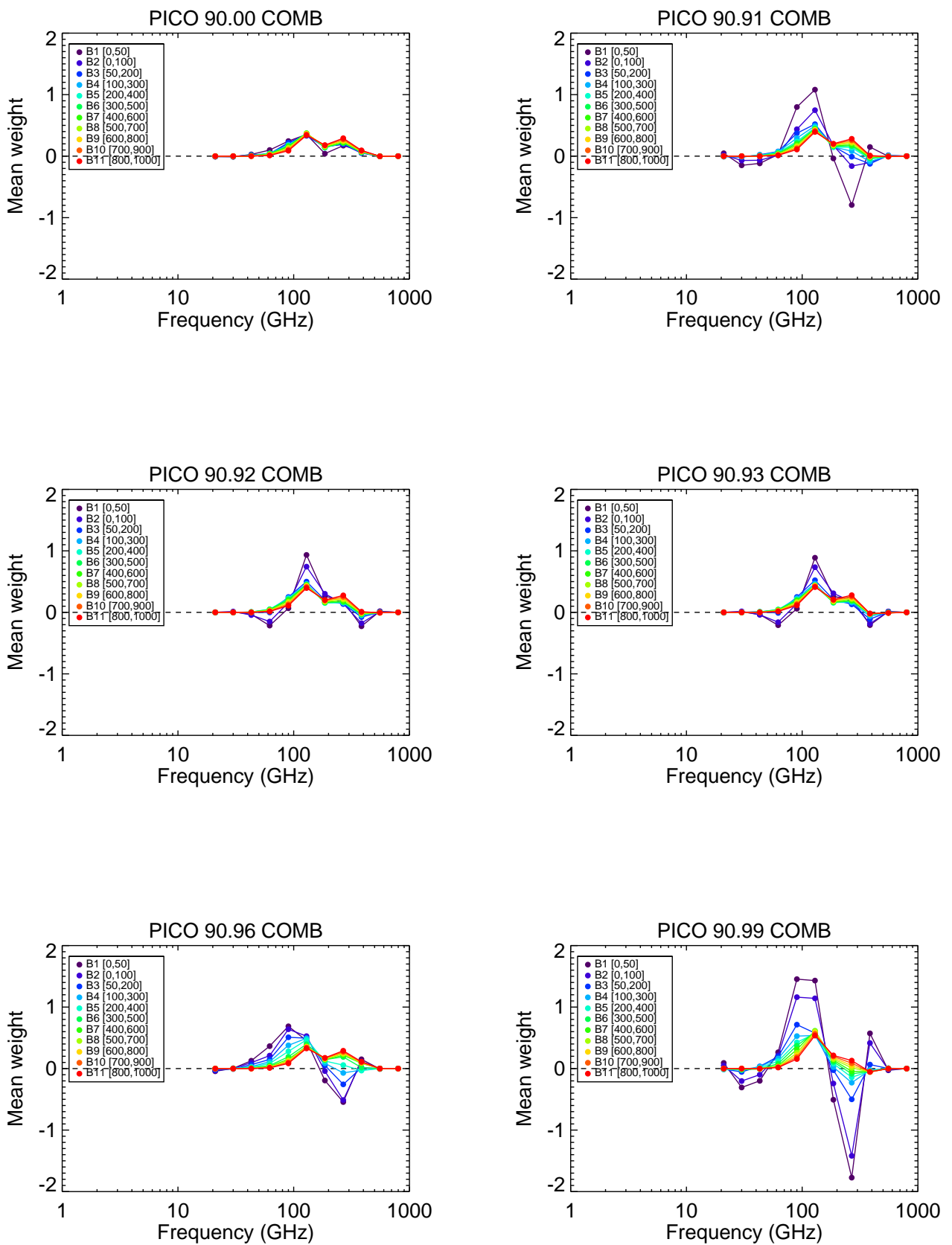
Band index	l_{min}	l_{peak}	l_{max}	n_{side}
1	0	0	50	32
2	0	50	100	64
3	50	100	200	128
4	100	200	300	256
5	200	300	400	256
6	300	400	500	256
7	400	500	600	512
8	500	600	700	512
9	600	700	800	512
10	700	800	900	512
11	800	900	1000	512

However, the reconstructed B-mode maps cannot be completely free from contamination by residual foregrounds and noise. Therefore, for further analysis, a set of conservative masks are derived from the residuals of foreground map. For the computation of the angular power spectrum of the high resolution NILC CMB maps, we use a pseudo-Cl estimator. Currently I am experimenting with different sets of confidence mask. Soon I will share with you the results obtained using those new mask.

2.5.3 PSM sky simulations at $N_{side} = 16$

The PSM (Planck Sky Model) [37] is a simulation software developed by the *Planck* Collaboration to model sky emissions at submillimetre to centimetre wavelengths based on the state-of-the-art observations of the *Planck* satellite mission and earlier surveys. We use the PSM to simulate all-sky polarization maps at the 21 frequency bands of *PICO* (21 to 800 GHz). The simulated components of emission include CMB E- and B-mode polarization, polarized Galactic synchrotron and thermal dust foreground emissions. The CMB template map is generated from CAMB [38] through CMB E- and B-mode power spectra by assuming an optical depth to reionization of $\tau = 0.06$ and a tensor-to-scalar ratio of $r = 10^{-3}$, as well as gravitational lensing effects. Galactic dust Q and U polarization maps are generated from the *Planck* GNILC dust intensity all-sky map at 353 GHz, in which cosmic infrared background (CIB), CMB, and noise have been filtered out, and assuming average polarization fractions of 5-10%. Galactic synchrotron Q and U maps are based on the *WMAP* polarization observations at 23 GHz [39].

The thermal dust Q and U template maps are extrapolated across *PICO* frequencies through a modified blackbody energy spectrum having variable spectral index and temperature over the sky, using the Planck GNILC dust spectral index and temperature maps for which $\beta_d = 1.6 \pm 0.1$ and $T_d = 19.4 \pm 1.3$ K, respectively. The synchrotron Q and U template maps are extrapolated across *PICO* frequencies through a curved power-law spectrum, with a variable spectral index over the sky of $\beta_s = -3 \pm 0.06$ based on the synchrotron index map from [39], and a constant curvature of $C_s = 0.3$ [40] to account for different populations of cosmic ray electrons and possible AME polarization [41]. The CMB, dust, and synchrotron component maps in each *PICO* frequency are



then co-added, and instrumental white noise is added to each sky map using the sensitivities per frequency quoted by *PICO*. The PSM simulations are generated at a pixel resolution of HEALPix [42] $N_{\text{side}} = 16$ ($2 \leq \ell \leq 47$), therefore assuming spectral variations of the foregrounds across $N_{\text{side}} = 16$ pixels.

2.5.4 PICO forecasts with COMMANDER

We have applied the COMMANDER algorithm [43] to the set of PSM $N_{\text{side}} = 16$ sky simulations for *PICO*. COMMANDER is a Bayesian parametric fitting method which has been thoroughly used by the *Planck* Collaboration for the separation of CMB and foreground components [44, 45]. Using MCMC Gibbs sampling in each pixel, the COMMANDER algorithm allows to fit simultaneously the amplitudes of CMB and foreground components, their spectral parameters, and the CMB E- and B-mode power spectra in a self-consistent Bayesian framework. A Blackwell-Rao estimator applied to the Gibbs samples allows in particular to reconstruct the statistical (chi-square) distribution of the CMB B-mode power spectrum at each multipole, and the posterior distribution of the tensor-to-scalar ratio [46, 47]. Such a Bayesian method performs end-to-end propagation of all foreground uncertainties towards the tensor-to-scalar ratio, while providing a chi-square goodness-of-fit in each pixel which allows to revise the parametric model or readjust the galactic mask a posteriori. The *PICO* sky maps are processed by COMMANDER using a Galactic mask leaving a 50% fraction of the sky, and forecasts on r are computed using the range of low multipoles $2 \leq \ell \leq 47$.

First considering *PICO* sky simulations *without foregrounds*, but just CMB and noise in the *PICO* frequency bands, we recover the tensor-to-scalar ratio with $\sigma(r = 10^{-3}) = 0.40 \times 10^{-3}$ significance: this provides the minimum uncertainty on $r = 10^{-3}$ that can be achieved by *PICO* from low multipoles $2 \leq \ell \leq 47$ in the absence of foregrounds on 50% of the sky. In the presence of foregrounds (full simulation), with variable spectral indices over the sky, the COMMANDER results on r are of similar quality due to the broad frequency range of *PICO* (21 -800 GHz), with $\sigma(r = 10^{-3}) = 0.41 \times 10^{-3}$ for *PICOv2-1.4* and $\sigma(r = 10^{-3}) = 0.36 \times 10^{-3}$ for *PICOv3* (increased sensitivities per channel) after foreground cleaning. Assuming now that 60% delensing in power has been achieved (modified PSM simulation with only 40% of the lensing B-mode power left in the CMB map realisation), the uncertainty on $r = 10^{-3}$ is improved by more than 30%, with $\sigma(r = 10^{-3}) = 0.24 \times 10^{-3}$ for *PICOv3* after foreground cleaning and 60% delensing. Finally, we note that discarding low- and high-frequency bands, resulting in a descoped version of *PICO* with a narrower frequency range of 43-462 GHz, the COMMANDER results are degraded by 75%, with an uncertainty increasing from $\sigma(r = 10^{-3}) = 0.4 \times 10^{-3}$ to $\sigma(r = 10^{-3}) = 0.7 \times 10^{-3}$ after foreground cleaning. The main reason for the degradation is a lack of constraining power on the dust temperature variations over the sky when discarding frequencies above 462 GHz, which translates into a degradation of the fitted CMB B-mode power spectrum by extrapolation towards central frequencies.

[MR: I can add a figure on COMMANDER C_ℓ^{BB} results with *PICO*, if needed]

We are working in parallel on COMMANDER2, a new version of the algorithm operating in harmonic space, thus allowing to perform the parametric fit at full resolution and to further reduce the uncertainty on r by the increase of information / modes.

2.6 Systematic Errors (3 pgs, Crill)

Aside from control of foregrounds, the most compelling reason to observe the CMB from space is the opportunity for control of systematic errors. The L2 environment offers excellent stability as well as the ability to observe large fractions of the sky on many time scales without interference from the Sun, Earth, or Moon. The redundancy of observations allows the checking of consistency of results and an improved ability to calibrate and to correct systematic errors in post-processing analysis.

A rich literature investigates the types of systematic errors due to the environment, the instrumentation, observation strategies, and data analysis that confound the polarization measurement by creating a bias or an increased variance[48, 49, 50]. Every measurement to date has reached a systematic error limit, and have advanced many sophisticated techniques to mitigate systematics, finding both new technological solutions and new analysis techniques. As an example, the BICEP’s systematics limited it to $r=0.1$ [?] while through additional effort within the program, BICEP2 achieved a systematics limit of $r=6 \times 10^{-3}$ [51]). In the near term, the ground based and suborbital CMB community will continue to develop new techniques in handling systematics, particularly in developing the CMB-S4 project.

All prior on-orbit measurements of CMB polarization were limited by systematic errors until an in-depth study of the systematics was performed and the post-processing data analysis suppressed them[10, 52, 53]. Particularly we note Fig. 3 of the Planck legacy paper which indicates Planck’s systematic error limits on the polarization power spectral measurements. Recently studied space missions, such as EPIC-IM, LiteBird and *CORE*, have placed systematic error mitigation at the forefront of the case for their mission and have developed tools and strategies for estimating and mitigating these[54, 55, 56].

End-to-end simulation of the experiment is an essential tool, including realistic instabilities and non-idealities of the spacecraft, telescope, instrument and folding in data post-processing techniques used to mitigate the effects. Systematics are coupled with the spacecraft scan strategy, and the details of the data analysis pipeline.

2.6.1 List of Systematics

The systematic errors faced by PICO can be categorized into three broad categories: 1) Intensity-to-polarization leakage, 2) stability, and 3) straylight and are listed in Table 2. These were prioritized for further study using a risk factor incorporating the working group’s assessment of how mission-limiting the effect is, how well these effects are understood by the community and whether mitigation techniques exist.

The three highest risk systematic errors were studied further and are discussed in subsections below. The PICO team used simulation and analysis tools developed for Planck[57] and *CORE*, adapting them for PICO.

2.6.2 Absolute polarization angle calibration

CMB polarization can be rotated due to 1. a birefringent primordial Universe, or a Faraday rotation due a primordial magnetic field [61], 2. birefringent foregrounds, or interaction with the Galactic magnetic field, 3. systematic effects in the instrument, and in particular an error on the direction of polarization measured by each detector. While the first two sources create a rotation that may depend on scale, position and/or frequency, the latter depends mainly on the detector.

Name	Risk	Description	State-of-the-art	Additional Mitigation Needed
Leakage				
Polarization Angle Calibration.....	5	Uncertainty in polarization calibration leaks $E \rightarrow B$.	Knowledge of astrophysical calibrators to 0.3° (author?) [58]; ground measurement to 0.9° reconstruction to 0.2° using TB and EB demonstrated by <i>Planck</i> [?]	See Sect. 2.6.2 for discussion.
Bandpass Mismatch.....	4	Edges and shapes of the spectral filters vary from detector to detector. leaks $T \rightarrow P$, $P \rightarrow P$ if the source's bandpass differs from calibrator's bandpass[?]	Precise bandpass measurement[?]; SRoll algorithm[?]; filtering technique[?]; additional component solution (see Banerji& Delabrouille in prep).	State-of-the-art meet requirements.
Beam mismatch	4	Beam shapes differ between detectors that are combined to reconstruct polarization; leaks $T \rightarrow P$, $P \rightarrow P$	See Sect. 2.6.2	State-of-the-art meet requirements.
Time Response Accuracy and Stability.....	4	Uncertainty of detector in time constants (measurement errors, time variability) biases polarization angle, pointing and beam size. In a constant spin-rate mission (PICO) is degenerate with the beam shape. leaks $T \rightarrow P$, $P \rightarrow P$	On-orbit reconstruction of time response to 0.1% across a wide signal band[59], residuals corrected as part of beam and map-making algorithm[?].	State-of-the-art meet requirements.
Readout Cross-talk.....	4	Power in one detector leaks into other detectors	<i>Planck</i> 's high-impedance bolometers with crosstalk measured at the level of 10^{-3} did not impact CMB polarization science[?]. Cross-talk low-impedance bolometers measured at XXX.	State-of-the-art meets requirements.
Chromatic beam shape	4	Beam shape is a function of source SED: measured using a planet, used to build a window function to correct CMB power spectrum.	<i>Planck</i> simulations and parameterization as part of the likelihood.	Should be further investigated in Phase A of a mission using physical optics simulations.
Gain mismatch	3	Relative gain between detectors that are combined to reconstruct polarization; error leaks $T \rightarrow P$	mission-average relative calibration demonstrated to 10^{-4} to 10^{-5} level [?]	State-of-the-art measurement of mission-average gain meets requirements; Sect. 2.6.3 describes effects of stability in time in relative gains.
Cross-polarization	3	$Q \rightarrow U$ rotation by the optical elements of the instrument.	Degenerate with polarization gain calibration.	State-of-the-art meets requirements.
Stability				
Gain Stability	5	Time-variation of detector gain due to time variability of detector heat sink temperature variations and optical loading.	Reconstruction of time variability of gain to 0.2% in <i>Planck</i> [?].	See Sect. 2.6.3; Gain fluctuations in PICO on the level of XXX% on time scales of YYY can be corrected in post-processing.
Pointing jitter.....	3	Random pointing error mixes T , E and B at small angular scale	Pointing reconstruction in <i>Planck</i> to XXX arcsec.	State-of-the-art meets requirements.
Straylight				
Far Sidelobes	5	Pickup of Galactic signals at large angles from the main beam axis; Spillover can be highly polarized.	<i>Planck</i> validated straylight model in anechoic chamber to -80 dBi[60].	Design of optical system and baffling, informed by telescope straylight simulations. See Sect. 2.6.4 for a study of beams calculated with a physical optics code for the PICO telescope and simulated Galactic pickup during the reference mission.
Other				
Residual correlated cosmic ray hits	3	detectors experience correlated cosmic ray hits below detection threshold resulting in misestimated noise covariance.	<i>Planck</i> /HFI found the 5% percent noise correlation due to this effect did not impact results[?].	State-of-the-art detector design to reduce cosmic ray cross-section; State-of-the-art analysis techniques (accounting for correlated noise) meet requirements.

Table 2: Systematic errors expected in PICO's measurement of CMB polarization.

A rotation α of the direction of polarization mixes the Q and U Stokes parameters via $Q \pm iU \longrightarrow e^{\mp i2\alpha}(Q \pm iU)$ and thus mixes the the power spectra and their correlations as illustrated in Fig. 9.

The most recent constraints on cosmological birefringence (**author?**) [64] were limited by uncertainties on the detector orientations. In Planck, the detectors were characterized pre-launch to

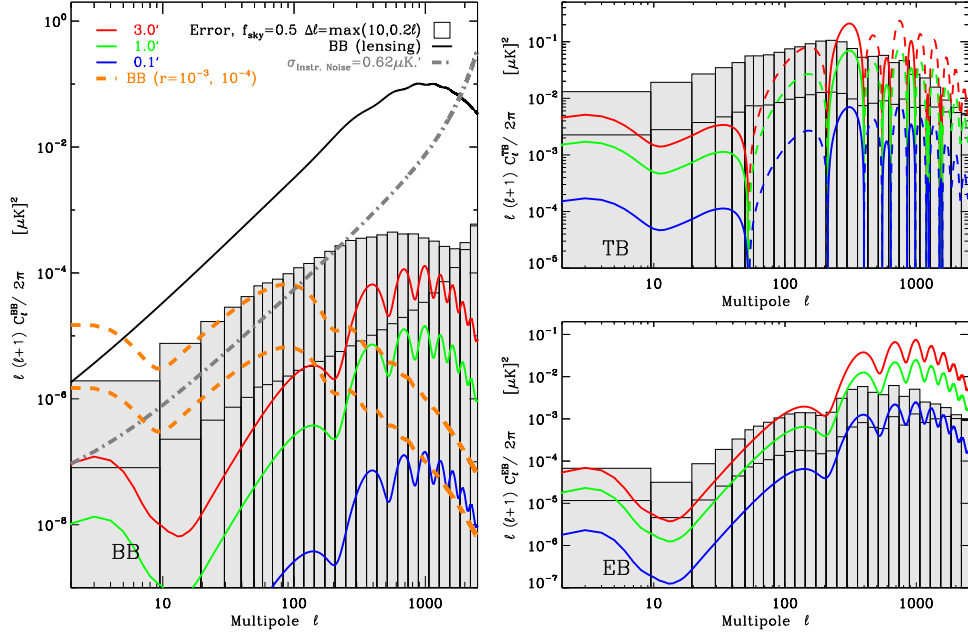


Figure 9: Effect of a rotation of the angle of polarization, assuming the Planck 2018 Λ -CDM best fit model [62] with $\tau = 0.054$ and expected PICO noise performance, assuming perfect delensing.

$\pm 0.9^\circ$ (rel.) $\pm 0.3^\circ$ (abs.) [63]. For PICO, the relative rotation of the detectors will be measured to a few $0.1'$ using the CMB, but the overall rotation is unlikely to be known pre-launch to better than Planck. Known polarized sources, such as the Crab Nebula, are not characterized well enough independently to serve as calibrators; (**author?**) [58] show that the current uncertainty of $0.33^\circ = 20'$ on the Crab polarization orientation, limits a B mode measurement to $r \sim 0.01$, far from PICO’s target.

In the absence of other systematics and foregrounds, a polarization rotation error α of $10'$ degrades the error bar of r by 30%, while EB , TB and BB spectra can measure a rotation α at 3σ when $\alpha \sim 0.07, 0.2$ and $0.9'$ respectively on perfectly delensed maps, and $0.25, 0.9$ and $4.5'$ on raw maps.

In principle, the technique of using the TB and EB spectra can detect and measure a global polarization rotation error at levels ($0.1'$) below those affecting r measurements in BB ($> 1'$). However, a future mission should simulate additional aspects, such as delensing, the interaction with foregrounds, and $1/f$ noise in simulating and assessing the impact of an angle calibration error.

2.6.3 Gain Stability

Photometric calibration is the process of converting the raw output of the receivers into astrophysical units via the characterization of the *gain factor* $G(t)$ which we allow to vary with time. In space, the characterization of $G(t)$ uses the dipole. For the PICO concept study, we evaluated the impact of noise in the estimation of $G(t)$ using the tools developed for the Planck/LFI instrument and the CORE mission proposal. The quality of the estimate depends on the noise level of the receivers, but also on the details of the scanning strategy. To analyze the impact of calibration uncertainties on PICO, we performed the following analysis:1. We simulated the observation of

the sky, assuming four receivers, the nominal scanning strategy, and $1/f$ noise. The simulated sky contained CMB anisotropies, plus the CMB dipole. 2. We ran the calibration code to fit the dipole against the raw data simulated during step 1. 3. We again simulated the observation of the sky, this time using the values of G computed during step 2, which contain errors due to the presence of noise and the CMB signal.

The presence of large-scale Galactic emission features can bias the estimation of calibration factors. Ideally, a full data analysis pipeline would pair the calibration step with the component separation step, following a schema similar to Planck/LFI’s legacy data processing [CITATION]: the calibration code is followed by a component separation analysis, and these two steps are iterated until the solution converges.

Results of the simulation (neglecting foregrounds) are shown in Figures XXX and YYY. The scanning strategy employed by PICO allows for a much better calibration than Planck, thanks to the much faster precession.

2.6.4 Far Sidelobe Pickup

Measurement of each detector’s response to signals off axis, which tends to be weak (-80dB less than the peak response) but spread over a very large solid angle, is difficult to do pre-launch, and may not even be done accurately after launch. Nonetheless, this far sidelobe can couple bright Galactic signal from many tens of degrees off-axis and confuse it with polarized signal from the CMB off the Galactic plane.

To evaluate this systematic error, GRASP software³ was used to compute the PICO telescope’s response over the full sky. This full-sky beam was convolved with a polarized Galactic signal and a full PICO mission scan using the simulation pipeline. The far sidelobe pickup was estimated to contribute less than XXX to the B-mode angular power spectrum and thus an error in r of YYY.

Due to the difficulties of measuring this beam, physical optics simulation capabilities must be maintained and validated as well as possible with on-orbit data.

2.6.5 Key Findings

Properly modeling, engineering for, and controlling the effects of systematic errors in a next-generation CMB probe is critical. As of today, we conclude that there is a clear path to demonstrate that state-of-the-art technology and data processing can take advantage of the L2 environment and control systematic errors to a level that enables the science goals of PICO. In particular we note:

- The raw sensitivity of the instrument should include enough margin that data subsets can independently achieve the science goals. This allows testing of the results in the data analysis and additional data cuts, if needed.
- NASA’s support of ground-based and suborbital CMB missions will mitigate risk to a future space mission as PICO by continuing to develop analysis techniques and technology for mitigation of systematic errors.
- In a PICO mission’s phase A, a complete end-to-end system-level simulation software facility would be developed to assist the team in setting requirements and conducting trades

³<https://www.ticra.com>

between subsystem requirements while realistically accounting for post-processing mitigation. Any future CMB mission is likely to have similar orbit and scan characteristics to those of PICO, thus there is an opportunity for NASA and the CMB community to invest in further development of this capability now.

2.7 Measurement Requirements (2 pgs, Hanany & Trangsrud)

The set of physical parameters and observables that derive from the PICO science objectives place requirements on the depth of the mission, the fraction of sky the instrument scans, the frequency range the instrument probes and the number of frequency bands, the angular resolution provided by the reflectors, and the specific pattern with which PICO will observe the sky. We discuss each of these aspects.

- **Depth** We quantify survey depth in terms of the RMS fluctuations that would give a signal-to-noise ratio of 1 on a sky pixel that is 1 arcminute on a side. Depth in any frequency band is determined by detector sensitivity, the number of detectors in the focal plane, the sky area covered, and the duration of the mission. The science objective driving the depth requirement is SO1, the search for the IGW signal which requires a depth of $0.87 \mu\text{K} \cdot \text{arcmin}$. This requirement is a combination of the low-level of the signal, the need to separate the various signals detected in each band, and the need to detect and subtract systematic effects to the required levels.

- **Sky Coverage** There are several science goals driving a full sky survey for PICO. The term ‘full sky’ refers to the entire area of sky available after separating other astrophysical sources of confusion. In practice this implies an area of 50-70% of the full sky for probing non-Galactic signals, and the rest of the sky for achieving the Galactic science goals.

(1) Probing the optical depth to the epoch of reionization (STM SO5) requires full sky coverage as the signal peaks in the EE power spectrum on angular scales of 20 to 90 degrees. Measuring this optical depth to limits imposed by the statics of the small number of available ℓ modes is crucial for minimizing the error on the neutrino mass measurement.

(2) If $r \neq 0$, the BB power spectrum due to IGW (STM SO1) also has a local maximum in the same range of angular scales (20 to 90 degrees). For $r \gtrsim 0.001$ (CHECK) this local maximum is at a higher level than the BB lensing spectrum, making this range of scales appealing to survey, as there is no need to separate the signatures of two cosmological signals.

(3) The PICO constraint on N_{eff} (STM SO4) requires a determination of the EE power spectrum to limits imposed by the statics of available ℓ modes. Full sky coverage is required to achieve this limit. (4) PICO’s survey of the Galactic plane and regions outside of it is essential to achieving its Galactic structure and star formation science goals (SO6, 7, 8).

- **Frequency Bands** The multitude of astrophysical signals that PICO will characterize determine the frequency range and number of sub-bands that PICO uses. The IGW signal peaks in the frequency range between 30 and 300 GHz. However, Galactic signals, which are themselves signals PICO strives to characterize, are a source of confusion for the IGW. The Galactic signals and the IGW are separable using their spectral signature. Simulations indicate that 21 bands, each with $\sim 25\%$ bandwidth, that are spread across the range of 20 - 800 GHz can achieve the separation at the level of fidelity required by PICO.

Characterizing the Galactic signals, specifically the make up of Galactic dust (SO7), requires spectral characterization of galactic dust in frequencies between 100 and 800 GHz. [Aren’t there synchrotron questions that are answerable with spectral information?](#)

- **Resolution** Several science objectives require an aperture of 1.5 m and the resolution listed

in Table ???. To reach $\sigma(r) = ??$ we will need to 'delens' the E- and B-mode maps that PICO will generate; see Section ???. Delensing is enabled with a map that has a native resolution of 2-3 arcminutes at frequencies between 100 and 300 GHz. Similar resolution is required to achieve the constraints on the number of light relics (SO??), which will be extracted from the EE power spectrum at multipoles $100 \lesssim \ell \lesssim 2500$. The process of delensing may be affected by other signals, primarily the signal due to Galactic dust. It is thus required to map Galactic dust to at least the same resolution as at 300 GHz. Higher resolution is mandated by science objectives 6,7, and 8, which require resolution of 1 arcminute at 800 GHz. We have thus chosen to implement diffracted limited resolution between 20 and 800 GHz.

- **Sky Scan Pattern** polarization systematics, 1/f noise

3 Instrument (6 pgs, Hanany & Trangsrud)

Telescope (Hanany / Young), focal plane (Hanany / Young), cooling (Trangsrud), readout (O'Brient)
Review: Bock, Hubmayr, Suzuki,

4 Mission (5 pgs, Trangsrud)

To be included: mission architecture, spacecraft and subsystems, orbit, attitude control and determination (Trangsrud)

5 Technology Maturation (4 pgs, O'Brient & Trangsrud)

Requirements, planned activities, schedules and milestones, estimated cost (O'Brient?)

For each technology include:

- Requirements
- Planned activities
- Schedule and Milestones
- Estimated Cost

6 Management, Risk, Heritage, and Cost (4 pgs, Trangsrud)

cost, risk, heritage (Trangsrud)

References

- [1] G. Steigman. Cosmology confronts particle physics. *Annual Review of Nuclear and Particle Science*, 29:313–338, 1979.
- [2] M. Bolz, A. Brandenburg, and W. Buchmuller. Thermal production of gravitinos. *Nucl. Phys.*, B606:518–544, 2001. [Erratum: Nucl. Phys.B790,336(2008)].
- [3] Christopher Brust, David E. Kaplan, and Matthew T. Walters. New Light Species and the CMB. *JHEP*, 12:058, 2013.
- [4] Daniel Baumann, Daniel Green, and Benjamin Wallisch. A New Target for Cosmic Axion Searches. *Phys. Rev. Lett.*, 117(17):171301, 2016.
- [5] Daniel Green, Joel Meyers, and Alexander van Engelen. CMB Delensing Beyond the B Modes. *ArXiv e-prints*, 2016.
- [6] Cora Dvorkin, Kfir Blum, and Marc Kamionkowski. Constraining Dark Matter-Baryon Scattering with Linear Cosmology. *Phys. Rev.*, D89(2):023519, 2014.
- [7] Francis-Yan Cyr-Racine, Roland de Putter, Alvise Raccanelli, and Kris Sigurdson. Constraints on Large-Scale Dark Acoustic Oscillations from Cosmology. *Phys. Rev.*, D89(6):063517, 2014.
- [8] Manuel A. Buen-Abad, Gustavo Marques-Tavares, and Martin Schmaltz. Non-Abelian dark matter and dark radiation. *Phys. Rev.*, D92(2):023531, 2015.
- [9] Julien Lesgourgues, Gustavo Marques-Tavares, and Martin Schmaltz. Evidence for dark matter interactions in cosmological precision data? *JCAP*, 1602(02):037, 2016.
- [10] Planck Collaboration, N. Aghanim, M. Ashdown, J. Aumont, C. Baccigalupi, M. Ballardini, A. J. Banday, R. B. Barreiro, N. Bartolo, S. Basak, R. Battye, K. Benabed, J.-P. Bernard, M. Bersanelli, P. Bielewicz, J. J. Bock, A. Bonaldi, L. Bonavera, J. R. Bond, J. Borrill, F. R. Bouchet, F. Boulanger, M. Bucher, C. Burigana, R. C. Butler, E. Calabrese, J.-F. Cardoso, J. Carron, A. Challinor, H. C. Chiang, L. P. L. Colombo, C. Combet, B. Comis, A. Coulais, B. P. Crill, A. Curto, F. Cuttaia, R. J. Davis, P. de Bernardis, A. de Rosa, G. de Zotti, J. Delabrouille, J.-M. Delouis, E. Di Valentino, C. Dickinson, J. M. Diego, O. Doré, M. Douspis, A. Ducout, X. Dupac, G. Efstathiou, F. Elsner, T. A. Enßlin, H. K. Eriksen, E. Falgarone, Y. Fantaye, F. Finelli, F. Forastieri, M. Frailis, A. A. Fraisse, E. Franceschi, A. Frolov, S. Galeotta, S. Galli, K. Ganga, R. T. Génova-Santos, M. Gerbino, T. Ghosh, J. González-Nuevo, K. M. Górski, S. Gratton, A. Gruppuso, J. E. Gudmundsson, F. K. Hansen, G. Helou, S. Henrot-Versillé, D. Herranz, E. Hivon, Z. Huang, S. Ilic, A. H. Jaffe, W. C. Jones, E. Keihänen, R. Keskitalo, T. S. Kisner, L. Knox, N. Krachmalnicoff, M. Kunz, H. Kurki-Suonio, G. Lagache, J.-M. Lamarre, M. Langer, A. Lasenby, M. Lattanzi, C. R. Lawrence, M. Le Jeune, J. P. Leahy, F. Levrier, M. Liguori, P. B. Lilje, M. López-Caniego, Y.-Z. Ma, J. F. Macías-Pérez, G. Maggio, A. Mangilli, M. Maris, P. G. Martin, E. Martínez-González, S. Matarrese, N. Mauri, J. D. McEwen, P. R. Meinhold, A. Melchiorri, A. Menella, M. Migliaccio, M.-A. Miville-Deschénes, D. Molinari, A. Moneti, L. Montier, G. Morganante, A. Moss, S. Mottet, P. Naselsky, P. Natoli, C. A. Oxborrow, L. Pagano, D. Paoletti,

- B. Partridge, G. Patanchon, L. Patrizii, O. Perdereau, L. Perotto, V. Pettorino, F. Piacentini, S. Plaszczynski, L. Polastri, G. Polenta, J.-L. Puget, J. P. Rachen, B. Racine, M. Reinecke, M. Remazeilles, A. Renzi, G. Rocha, M. Rossetti, G. Roudier, J. A. Rubiño-Martín, B. Ruiz-Granados, L. Salvati, M. Sandri, M. Savelainen, D. Scott, G. Sirri, R. Sunyaev, A.-S. Suur-Uski, J. A. Tauber, M. Tenti, L. Toffolatti, M. Tomasi, M. Tristram, T. Trombetti, J. Valiviita, F. Van Tent, L. Vibert, P. Vielva, F. Villa, N. Vittorio, B. D. Wandelt, R. Watson, I. K. Wehus, M. White, A. Zacchei, and A. Zonca. Planck intermediate results. XLVI. Reduction of large-scale systematic effects in HFI polarization maps and estimation of the reionization optical depth. *ArXiv e-prints*, May 2016.
- [11] Manoj Kaplinghat, Lloyd Knox, and Yong-Seon Song. Determining neutrino mass from the CMB alone. *Phys. Rev. Lett.*, 91:241301, 2003.
- [12] Michael Levi et al. The DESI Experiment, a whitepaper for Snowmass 2013. *ArXiv e-prints*, 2013.
- [13] C. M. Hirata, S. Ho, N. Padmanabhan, U. Seljak, and N. A. Bahcall. Correlation of CMB with large-scale structure. II. Weak lensing. *Phys. Rev. D.*, 78(4):043520, August 2008.
- [14] Planck Collaboration, N. Aghanim, Y. Akrami, M. Ashdown, J. Aumont, C. Baccigalupi, M. Ballardini, A. J. Banday, R. B. Barreiro, N. Bartolo, S. Basak, K. Benabed, J.-P. Bernard, M. Bersanelli, P. Bielewicz, J. J. Bock, J. R. Bond, J. Borrill, F. R. Bouchet, F. Boulanger, M. Bucher, C. Burigana, E. Calabrese, J.-F. Cardoso, J. Carron, A. Challinor, H. C. Chiang, L. P. L. Colombo, C. Combet, B. P. Crill, F. Cuttaia, P. de Bernardis, G. de Zotti, J. Delabrouille, E. Di Valentino, J. M. Diego, O. Doré, M. Douspis, A. Ducout, X. Dupac, G. Efstathiou, F. Elsner, T. A. Enßlin, H. K. Eriksen, Y. Fantaye, R. Fernandez-Cobos, F. Forastieri, M. Frailis, A. A. Fraisse, E. Franceschi, A. Frolov, S. Galeotta, S. Galli, K. Ganga, R. T. Génova-Santos, M. Gerbino, T. Ghosh, J. González-Nuevo, K. M. Górski, S. Gratton, A. Gruppuso, J. E. Gudmundsson, J. Hamann, W. Handley, F. K. Hansen, D. Herranz, E. Hivon, Z. Huang, A. H. Jaffe, W. C. Jones, A. Karakci, E. Keihänen, R. Keskitalo, K. Kiiveri, J. Kim, L. Knox, N. Krachmalnicoff, M. Kunz, H. Kurki-Suonio, G. Lagache, J.-M. Lamarre, A. Lasenby, M. Lattanzi, C. R. Lawrence, M. Le Jeune, F. Levrier, A. Lewis, M. Liguori, P. B. Lilje, V. Lindholm, M. López-Caniego, P. M. Lubin, Y.-Z. Ma, J. F. Macías-Pérez, G. Maggio, D. Maino, N. Mandolesi, A. Mangilli, A. Marcos-Caballero, M. Maris, P. G. Martin, E. Martínez-González, S. Matarrese, N. Mauri, J. D. McEwen, A. Melchiorri, A. Mennella, M. Migliaccio, M.-A. Miville-Deschénes, D. Molinari, A. Moneti, L. Montier, G. Morgante, A. Moss, P. Natoli, L. Pagano, D. Paoletti, B. Partridge, G. Patanchon, F. Perrotta, V. Pettorino, F. Piacentini, L. Polastri, G. Polenta, J.-L. Puget, J. P. Rachen, M. Reinecke, M. Remazeilles, A. Renzi, G. Rocha, C. Rosset, G. Roudier, J. A. Rubiño-Martín, B. Ruiz-Granados, L. Salvati, M. Sandri, M. Savelainen, D. Scott, C. Sirignano, R. Sunyaev, A.-S. Suur-Uski, J. A. Tauber, D. Tavagnacco, M. Tenti, L. Toffolatti, M. Tomasi, T. Trombetti, J. Valiviita, B. Van Tent, P. Vielva, F. Villa, N. Vittorio, B. D. Wandelt, I. K. Wehus, M. White, S. D. M. White, A. Zacchei, and A. Zonca. Planck 2018 results. VIII. Gravitational lensing. *ArXiv e-prints*, July 2018.
- [15] U. Seljak and C. M. Hirata. Gravitational lensing as a contaminant of the gravity wave signal in the CMB. *Phys. Rev. D.*, 69(4):043005, February 2004.

- [16] K. M. Smith, D. Hanson, M. LoVerde, C. M. Hirata, and O. Zahn. Delensing CMB polarization with external datasets. *JCAP*, 6:014, June 2012.
- [17] Planck Collaboration XXVI. Planck 2015 results. XXVI. The Second Planck Catalogue of Compact Sources. *Astron. Astrophys.*, 594:A26, September 2016.
- [18] M. Negrello, S. Amber, A. Amvrosiadis, Z.-Y. Cai, A. Lapi, J. Gonzalez-Nuevo, G. De Zotti, C. Furlanetto, S. J. Maddox, M. Allen, T. Bakx, R. S. Bussmann, A. Cooray, G. Covone, L. Danese, H. Dannerbauer, H. Fu, J. Greenslade, M. Gurwell, R. Hopwood, L. V. E. Koopmans, N. Napolitano, H. Nayyeri, A. Omont, C. E. Petrillo, D. A. Riechers, S. Serjeant, C. Tortora, E. Valiante, G. Verdoes Kleijn, G. Vernardos, J. L. Wardlow, M. Baes, A. J. Baker, N. Bourne, D. Clements, S. M. Crawford, S. Dye, L. Dunne, S. Eales, R. J. Ivison, L. Marchetti, M. J. Michałowski, M. W. L. Smith, M. Vaccari, and P. van der Werf. The Herschel-ATLAS: a sample of 500 μm -selected lensed galaxies over 600 deg². *MNRAS*, 465:3558–3580, March 2017.
- [19] F. Combes, M. Rex, T. D. Rawle, E. Egami, F. Boone, I. Smail, J. Richard, R. J. Ivison, M. Gurwell, C. M. Casey, A. Omont, A. Berciano Alba, M. Dessauges-Zavadsky, A. C. Edge, G. G. Fazio, J.-P. Kneib, N. Okabe, R. Pelló, P. G. Pérez-González, D. Schaefer, G. P. Smith, A. M. Swinbank, and P. van der Werf. A bright $z = 5.2$ lensed submillimeter galaxy in the field of Abell 773. *HLSJ091828.6+514223. Astron. Astrophys.*, 538:L4, February 2012.
- [20] T. Treu. Strong Lensing by Galaxies. *Ann. Rev. Astr. Ap.*, 48:87–125, September 2010.
- [21] R. Cañameras, N. P. H. Nesvadba, D. Guery, T. McKenzie, S. König, G. Petitpas, H. Dole, B. Frye, I. Flores-Cacho, L. Montier, M. Negrello, A. Beelen, F. Boone, D. Dicken, G. Lagache, E. Le Floc'h, B. Altieri, M. Béthermin, R. Chary, G. de Zotti, M. Giard, R. Kneissl, M. Krips, S. Malhotra, C. Martinache, A. Omont, E. Pointecouteau, J.-L. Puget, D. Scott, G. Soucail, I. Valtchanov, N. Welikala, and L. Yan. Planck's dusty GEMS: The brightest gravitationally lensed galaxies discovered with the Planck all-sky survey. *Astron. Astrophys.*, 581:A105, September 2015.
- [22] R. Cañameras, N. Nesvadba, R. Kneissl, B. Frye, R. Gavazzi, S. Koenig, E. Le Floc'h, M. Limousin, I. Oteo, and D. Scott. Planck's dusty GEMS. IV. Star formation and feedback in a maximum starburst at $z = 3$ seen at 60-pc resolution. *Astron. Astrophys.*, 604:A117, August 2017.
- [23] R. Cañameras, N. P. H. Nesvadba, R. Kneissl, M. Limousin, R. Gavazzi, D. Scott, H. Dole, B. Frye, S. Koenig, E. Le Floc'h, and I. Oteo. Planck's dusty GEMS. III. A massive lensing galaxy with a bottom-heavy stellar initial mass function at $z = 1.5$. *Astron. Astrophys.*, 600:L3, April 2017.
- [24] M. Rowan-Robinson, W. Saunders, A. Lawrence, and K. Leech. The QMW IRAS galaxy catalogue - A highly complete and reliable IRAS 60-micron galaxy catalogue. *MNRAS*, 253:485–495, December 1991.
- [25] Planck Collaboration XVI. Planck early results. XVI. The Planck view of nearby galaxies. *Astron. Astrophys.*, 536:A16, December 2011.

- [26] R. J. Ivison, A. M. Swinbank, I. Smail, A. I. Harris, R. S. Bussmann, A. Cooray, P. Cox, H. Fu, A. Kovács, M. Krips, D. Narayanan, M. Negrello, R. Neri, J. Peñarrubia, J. Richard, D. A. Riechers, K. Rowlands, J. G. Staguhn, T. A. Targett, S. Amber, A. J. Baker, N. Bourne, F. Bertoldi, M. Bremer, J. A. Calanog, D. L. Clements, H. Dannerbauer, A. Dariush, G. De Zotti, L. Dunne, S. A. Eales, D. Farrah, S. Fleuren, A. Franceschini, J. E. Geach, R. D. George, J. C. Helly, R. Hopwood, E. Ibar, M. J. Jarvis, J.-P. Kneib, S. Maddox, A. Omont, D. Scott, S. Serjeant, M. W. L. Smith, M. A. Thompson, E. Valiante, I. Valtchanov, J. Vieira, and P. van der Werf. Herschel-ATLAS: A Binary HyLIRG Pinpointing a Cluster of Starbursting Protoellipticals. *Ap. J.*, 772:137, August 2013.
- [27] T. Wang, D. Elbaz, E. Daddi, A. Finoguenov, D. Liu, C. Schreiber, S. Martín, V. Strazzullo, F. Valentino, R. van der Burg, A. Zanella, L. Ciesla, R. Gobat, A. Le Brun, M. Pannella, M. Sargent, X. Shu, Q. Tan, N. Cappelluti, and Y. Li. Discovery of a Galaxy Cluster with a Violently Starbursting Core at $z = 2.506$. *Ap. J.*, 828:56, September 2016.
- [28] I. Oteo, R. J. Ivison, L. Dunne, A. Manilla-Robles, S. Maddox, A. J. R. Lewis, G. de Zotti, M. Bremer, D. L. Clements, A. Cooray, H. Dannerbauer, S. Eales, J. Greenslade, A. Omont, I. Pérez-Fournón, D. Riechers, D. Scott, P. van der Werf, A. Weiss, and Z.-Y. Zhang. An Extreme Protocluster of Luminous Dusty Starbursts in the Early Universe. *Ap. J.*, 856:72, March 2018.
- [29] M. Negrello, J. Gonzalez-Nuevo, G. De Zotti, M. Bonato, Z.-Y. Cai, D. Clements, L. Danese, H. Dole, J. Greenslade, A. Lapi, and L. Montier. On the statistics of proto-cluster candidates detected in the Planck all-sky survey. *ArXiv e-prints*, May 2017.
- [30] R. A. Overzier. The realm of the galaxy protoclusters. A review. *Astron. Astrophys. Rev.*, 24:14, November 2016.
- [31] Planck Collaboration XXXIX. Planck intermediate results. XXXIX. The Planck list of high-redshift source candidates. *Astron. Astrophys.*, 596:A100, December 2016.
- [32] S. Alberts, A. Pope, M. Brodwin, D. W. Atlee, Y.-T. Lin, A. Dey, P. R. M. Eisenhardt, D. P. Gettings, A. H. Gonzalez, B. T. Jannuzzi, C. L. Mancone, J. Moustakas, G. F. Snyder, S. A. Stanford, D. Stern, B. J. Weiner, and G. R. Zeimann. The evolution of dust-obscured star formation activity in galaxy clusters relative to the field over the last 9 billion years. *MNRAS*, 437:437–457, January 2014.
- [33] G. Ghisellini, L. Foschini, M. Volonteri, G. Ghirlanda, F. Haardt, D. Burlon, and F. Tavecchio. The blazar S5 0014+813: a real or apparent monster? *MNRAS*, 399:L24–L28, October 2009.
- [34] R. W. Romani, D. Sowards-Emmerd, L. Greenhill, and P. Michelson. Q0906+6930: The Highest Redshift Blazar. *Ap. J. Lett.*, 610:L9–L11, July 2004.
- [35] G. Ghisellini, G. Tagliaferri, T. Sbarato, and N. Gehrels. SDSS J013127.34-032100.1: a candidate blazar with an 11 billion solar mass black hole at $z = 5.18$. *MNRAS*, 450:L34–L38, June 2015.
- [36] B. D. Metzger, P. K. G. Williams, and E. Berger. Extragalactic Synchrotron Transients in the Era of Wide-field Radio Surveys. I. Detection Rates and Light Curve Characteristics. *Ap. J.*, 806:224, June 2015.

- [37] J. Delabrouille, M. Betoule, J.-B. Melin, M.-A. Miville-Deschénes, J. Gonzalez-Nuevo, M. Le Jeune, G. Castex, G. de Zotti, S. Basak, M. Ashdown, J. Aumont, C. Baccigalupi, A. J. Banday, J.-P. Bernard, F. R. Bouchet, D. L. Clements, A. da Silva, C. Dickinson, F. Dodu, K. Dolag, F. Elsner, L. Fauvet, G. Faÿ, G. Giardino, S. Leach, J. Lesgourgues, M. Liguori, J. F. Macías-Pérez, M. Massardi, S. Matarrese, P. Mazzotta, L. Montier, S. Mottet, R. Paladini, B. Partridge, R. Piffaretti, G. Prezeau, S. Prunet, S. Ricciardi, M. Roman, B. Schaefer, and L. Toffolatti. The pre-launch Planck Sky Model: a model of sky emission at submillimetre to centimetre wavelengths. *Astron. Astrophys.*, 553:A96, May 2013.
- [38] A. Lewis, A. Challinor, and A. Lasenby. Efficient Computation of Cosmic Microwave Background Anisotropies in Closed Friedmann-Robertson-Walker Models. *Ap. J.*, 538:473–476, August 2000.
- [39] M.-A. Miville-Deschénes, N. Ysard, A. Lavabre, N. Ponthieu, J. F. Macías-Pérez, J. Aumont, and J. P. Bernard. Separation of anomalous and synchrotron emissions using WMAP polarization data. *Astron. Astrophys.*, 490:1093–1102, November 2008.
- [40] A. Kogut, J. Dunkley, C. L. Bennett, O. Doré, B. Gold, M. Halpern, G. Hinshaw, N. Jarosik, E. Komatsu, M. R. Nolta, N. Odegard, L. Page, D. N. Spergel, G. S. Tucker, J. L. Weiland, E. Wollack, and E. L. Wright. Three-Year Wilkinson Microwave Anisotropy Probe (WMAP) Observations: Foreground Polarization. *Ap. J.*, 665:355–362, August 2007.
- [41] C. Dickinson, Y. Ali-Haïmoud, A. Barr, E. S. Battistelli, A. Bell, L. Bernstein, S. Casassus, K. Cleary, B. T. Draine, R. Génova-Santos, S. E. Harper, B. Hensley, J. Hill-Valler, T. Hoang, F. P. Israel, L. Jew, A. Lazarian, J. P. Leahy, J. Leech, C. H. López-Caraballo, I. McDonald, E. J. Murphy, T. Onaka, R. Paladini, M. W. Peel, Y. Perrott, F. Poidevin, A. C. S. Readhead, J.-A. Rubiño-Martín, A. C. Taylor, C. T. Tibbs, M. Todorović, and M. Vidal. The State-of-Play of Anomalous Microwave Emission (AME) research. *New Ast. Rev.*, 80:1–28, February 2018.
- [42] K. M. Górski, E. Hivon, A. J. Banday, B. D. Wandelt, F. K. Hansen, M. Reinecke, and M. Bartelmann. HEALPix: A Framework for High-Resolution Discretization and Fast Analysis of Data Distributed on the Sphere. *Ap. J.*, 622:759–771, April 2005.
- [43] H. K. Eriksen, J. B. Jewell, C. Dickinson, A. J. Banday, K. M. Górski, and C. R. Lawrence. Joint Bayesian Component Separation and CMB Power Spectrum Estimation. *Ap. J.*, 676:10–32, March 2008.
- [44] Planck Collaboration, R. Adam, P. A. R. Ade, N. Aghanim, M. I. R. Alves, M. Arnaud, M. Ashdown, J. Aumont, C. Baccigalupi, A. J. Banday, and et al. Planck 2015 results. X. Diffuse component separation: Foreground maps. *Astron. Astrophys.*, 594:A10, September 2016.
- [45] Planck Collaboration, Y. Akrami, M. Ashdown, J. Aumont, C. Baccigalupi, M. Ballardini, A. J. Banday, R. B. Barreiro, N. Bartolo, S. Basak, K. Benabed, M. Bersanelli, P. Bielewicz, J. R. Bond, J. Borrill, F. R. Bouchet, F. Boulanger, M. Bucher, C. Burigana, E. Calabrese, J.-F. Cardoso, J. Carron, B. Casaponsa, A. Challinor, L. P. L. Colombo, C. Combet, B. P. Crill, F. Cuttaia, P. de Bernardis, A. de Rosa, G. de Zotti, J. Delabrouille, J.-M. Delouis,

E. Di Valentino, C. Dickinson, J. M. Diego, S. Donzelli, O. Doré, A. Ducout, X. Dupac, G. Efstathiou, F. Elsner, T. A. Enßlin, H. K. Eriksen, E. Falgarone, R. Fernandez-Cobos, F. Finelli, F. Forastieri, M. Frailis, A. A. Fraisse, E. Franceschi, A. Frolov, S. Galeotta, S. Galli, K. Ganga, R. T. Génova-Santos, M. Gerbino, T. Ghosh, J. González-Nuevo, K. M. Górski, S. Gratton, A. Gruppuso, J. E. Gudmundsson, W. Handley, F. K. Hansen, G. Helou, D. Herranz, Z. Huang, A. H. Jaffe, A. Karakci, E. Keihänen, R. Keskitalo, K. Kiiveri, J. Kim, T. S. Kisner, N. Krachmalnicoff, M. Kunz, H. Kurki-Suonio, G. Lagache, J.-M. Lamarre, A. Lasenby, M. Lattanzi, C. R. Lawrence, M. Le Jeune, F. Levrier, M. Liguori, P. B. Lilje, V. Lindholm, M. López-Caniego, P. M. Lubin, Y.-Z. Ma, J. F. Macías-Pérez, G. Maggio, D. Maino, N. Mandolesi, A. Mangilli, A. Marcos-Caballero, P. G. Martin, E. Martínez-González, S. Matarrese, N. Mauri, J. D. McEwen, P. R. Meinhold, A. Melchiorri, A. Mennella, M. Migliaccio, M.-A. Miville-Deschénes, D. Molinari, A. Moneti, L. Montier, G. Morgante, P. Natoli, F. Oppizzi, L. Pagano, D. Paoletti, B. Partridge, M. Peel, V. Pettorino, F. Piacentini, G. Polenta, J.-L. Puget, J. P. Rachen, M. Reinecke, M. Remazeilles, A. Renzi, G. Rocha, G. Roudier, J. A. Rubiño-Martín, B. Ruiz-Granados, L. Salvati, M. Sandri, M. Savelainen, D. Scott, D. S. Seljebotn, C. Sirignano, L. D. Spencer, A.-S. Suur-Uski, J. A. Tauber, D. Tavagnacco, M. Tenti, H. Thommesen, L. Toffolatti, M. Tomasi, T. Trombetti, J. Valiviita, B. Van Tent, P. Vielva, F. Villa, N. Vittorio, B. D. Wandelt, I. K. Wehus, A. Zacchei, and A. Zonca. Planck 2018 results. IV. Diffuse component separation. *ArXiv e-prints*, July 2018.

- [46] M. Remazeilles, C. Dickinson, H. K. K. Eriksen, and I. K. Wehus. Sensitivity and foreground modelling for large-scale cosmic microwave background B-mode polarization satellite missions. *MNRAS*, 458:2032–2050, May 2016.
- [47] M. Remazeilles, C. Dickinson, H. K. Eriksen, and I. K. Wehus. Joint Bayesian estimation of tensor and lensing B modes in the power spectrum of CMB polarization data. *MNRAS*, 474:3889–3897, March 2018.
- [48] W. Hu, M. M. Hedman, and M. Zaldarriaga. Benchmark parameters for CMB polarization experiments. *Phys. Rev. D.*, 67:043004–+, February 2003. astro-ph/0210096.
- [49] M. Shimon, B. Keating, N. Ponthieu, and E. Hivon. CMB polarization systematics due to beam asymmetry: Impact on inflationary science. *Phys. Rev. D.*, 77(8):083003–+, April 2008.
- [50] A. P. S. Yadav, M. Su, and M. Zaldarriaga. Primordial B-mode diagnostics and self-calibrating the CMB polarization. *Phys. Rev. D.*, 81(6):063512–+, March 2010.
- [51] Bicep2 Collaboration, P. A. R. Ade, R. W. Aikin, D. Barkats, S. J. Benton, C. A. Bischoff, J. J. Bock, J. A. Brevik, I. Buder, E. Bullock, C. D. Dowell, L. Duband, J. P. Filippini, S. Fliescher, S. R. Golwala, M. Halpern, M. Hasselfield, S. R. Hildebrandt, G. C. Hilton, K. D. Irwin, K. S. Karkare, J. P. Kaufman, B. G. Keating, S. A. Kernasovskiy, J. M. Kovac, C. L. Kuo, E. M. Leitch, M. Lueker, C. B. Netterfield, H. T. Nguyen, R. O'Brient, R. W. Ogburn, IV, A. Orlando, C. Pryke, S. Richter, R. Schwarz, C. D. Sheehy, Z. K. Staniszewski, R. V. Sudiwala, G. P. Teply, J. E. Tolan, A. D. Turner, A. G. Vieregg, C. L. Wong, and K. W. Yoon. Bicep2 III: Instrumental Systematics. *Ap. J.*, 814:110, December 2015.

- [52] C. L. Bennett, D. Larson, J. L. Weiland, N. Jarosik, G. Hinshaw, N. Odegard, K. M. Smith, R. S. Hill, B. Gold, M. Halpern, E. Komatsu, M. R. Nolta, L. Page, D. N. Spergel, E. Wollack, J. Dunkley, A. Kogut, M. Limon, S. S. Meyer, G. S. Tucker, and E. L. Wright. Nine-year Wilkinson Microwave Anisotropy Probe (WMAP) Observations: Final Maps and Results. *The Astrophysical Journal Supplement Series*, 208:20, October 2013.
- [53] Planck 2018-I. Planck 2018 results. I. Overview and the Cosmological Legacy of Planck. July 2018.
- [54] M. Hazumi, J. Borrill, Y. Chinone, M. A. Dobbs, H. Fuke, A. Ghribi, M. Hasegawa, K. Hattori, M. Hattori, W. L. Holzapfel, Y. Inoue, K. Ishidoshiro, H. Ishino, K. Karatsu, N. Katayama, I. Kawano, A. Kibayashi, Y. Kibe, N. Kimura, K. Koga, E. Komatsu, A. T. Lee, H. Matsuhara, T. Matsumura, S. Mima, K. Mitsuda, H. Morii, S. Murayama, M. Nagai, R. Nagata, S. Nakamura, K. Natsume, H. Nishino, A. Noda, T. Noguchi, I. Ohta, C. Otani, P. L. Richards, S. Sakai, N. Sato, Y. Sato, Y. Sekimoto, A. Shimizu, K. Shinozaki, H. Sugita, A. Suzuki, T. Suzuki, O. Tajima, S. Takada, Y. Takagi, Y. Takei, T. Tomaru, Y. Uzawa, H. Watanabe, N. Yamasaki, M. Yoshida, T. Yoshida, and K. Yotsumoto. LiteBIRD: a small satellite for the study of B-mode polarization and inflation from cosmic background radiation detection. In *Space Telescopes and Instrumentation 2012: Optical, Infrared, and Millimeter Wave*, volume 8442, page 844219, September 2012.
- [55] C. G. R. Wallis, M. L. Brown, R. A. Battye, and J. Delabrouille. Optimal scan strategies for future CMB satellite experiments. *Monthly Notices of the Royal Astronomical Society*, 466(1):425–442, 2017.
- [56] P. Natoli, M. Ashdown, R. Banerji, J. Borrill, A. Buzzelli, G. de Gasperis, J. Delabrouille, E. Hivon, D. Molinari, G. Patanchon, L. Polastri, M. Tomasi, F. R. Bouchet, S. Henrot-Versillé, D. T. Hoang, R. Keskitalo, K. Kiiveri, T. Kisner, V. Lindholm, D. McCarthy, F. Piacentini, O. Perdereau, G. Polenta, M. Tristram, A. Achucarro, P. Ade, R. Allison, C. Baccigalupi, M. Ballardini, A. J. Banday, J. Bartlett, N. Bartolo, S. Basak, D. Baumann, M. Bersanelli, A. Bonaldi, M. Bonato, F. Boulanger, T. Brinckmann, M. Bucher, C. Burigana, Z. Y. Cai, M. Calvo, C. S. Carvalho, M. G. Castellano, A. Challinor, J. Chluba, S. Clesse, I. Colantoni, A. Coppolecchia, M. Crook, G. D’Alessandro, P. de Bernardis, G. De Zotti, E. Di Valentino, J. M. Diego, J. Errard, S. Feeney, R. Fernandez-Cobos, F. Finelli, F. Forastieri, S. Galli, R. Genova-Santos, M. Gerbino, J. González-Nuevo, S. Grandis, J. Greenslade, A. Gruppuso, S. Hagstotz, S. Hanany, W. Handley, C. Hernandez-Monteagudo, C. Hervías-Caimapo, M. Hills, E. Keihänen, T. Kitching, M. Kunz, H. Kurki-Suonio, L. Lamagna, A. Lasenby, M. Lattanzi, J. Lesgourgues, A. Lewis, M. Liguori, M. López-Caniego, G. Luzzi, B. Maffei, N. Mandolesi, E. Martínez-González, C. J. A. P. Martins, S. Masi, S. Matarrese, A. Melchiorri, J. B. Melin, M. Migliaccio, A. Monfardini, M. Negrello, A. Notari, L. Pagano, A. Paiella, D. Paoletti, M. Piat, G. Pisano, A. Pollo, V. Poulin, M. Quartin, M. Remazeilles, M. Roman, G. Rossi, J. A. Rubino- Martin, L. Salvati, G. Signorelli, A. Tartari, D. Tramonte, N. Trappe, T. Trombetti, C. Tucker, J. Valiviita, R. Van de Weijgaert, B. van Tent, V. Vennin, P. Vielva, N. Vittorio, C. Wallis, K. Young, and M. Zannoni. Exploring cosmic origins with CORE: Mitigation of systematic effects. *Journal of Cosmology and Astro-Particle Physics*, 2018:022, April 2018.

- [57] Planck Collaboration, P. A. R. Ade, N. Aghanim, M. Arnaud, M. Ashdown, J. Aumont, C. Baccigalupi, A. J. Banday, R. B. Barreiro, J. G. Bartlett, and et al. Planck 2015 results. XII. Full focal plane simulations. *Astron. Astrophys.*, 594:A12, September 2016.
- [58] Jonathan Aumont, Juan-Francisco Macias-Perez, Alessia Ritacco, Nicolas Ponthieu, and Anna Mangilli. Absolute calibration of the polarisation angle for future CMB B -mode experiments from current and future measurements of the Crab nebula. May 2018.
- [59] P A R Planck Collaboration: Ade, N Aghanim, C Armitage-Caplan, M Arnaud, M Ashdown, F Atrio-Barandela, J Aumont, C Baccigalupi, A J Banday, R B Barreiro, E Battaner, K Benabed, A Benoît, A Benoit-Lévy, J P Bernard, M Bersanelli, P Bielewicz, J Bobin, J J Bock, J R Bond, J Borrill, F R Bouchet, J W Bowyer, M Bridges, M Bucher, C Burigana, J F Cardoso, A Catalano, A Challinor, A Chamballu, R R Chary, L Y Chiang, H C Chiang, P R Christensen, S Church, D L Clements, S Colombi, L P L Colombo, F Couchot, A Coulais, B P Crill, A Curto, F Cuttaia, L Danese, R D Davies, P de Bernardis, A de Rosa, G de Zotti, J Delabrouille, J M Delouis, F X Désert, J M Diego, H Dole, S Donzelli, O Dore, M Douspis, J Dunkley, X Dupac, G Efstathiou, T A Enßlin, H K Eriksen, F Finelli, O Forni, M Frailis, A A Fraisse, E Franceschi, S Galeotta, K Ganga, M Giard, Y Giraud-Héraud, J González-Nuevo, K M Gorski, S Gratton, A Gregorio, A Gruppuso, J E Gudmundsson, J Haissinski, F K Hansen, D Hanson, D Harrison, S Henrot-Versillé, C Hernandez-Monteagudo, D Herranz, S R Hildebrandt, E Hivon, M Hobson, W A Holmes, A Hornstrup, Z Hou, W Hovest, K M Huffenberger, T R Jaffe, A H Jaffe, W C Jones, M Juvela, E Keihänen, R Keskitalo, T S Kisner, R Kneissl, J Knoche, L Knox, M Kunz, H Kurki-Suonio, G Lagache, J M Lamarre, A Lasenby, R J Laureijs, C R Lawrence, R Leonardi, C Leroy, J Lesgourgues, M Liguori, P B Lilje, M Linden-Vørnle, M López-Caniego, P M Lubin, J F Macías-Pérez, C J MacTavish, B Maffei, N Mandolesi, M Maris, D J Marshall, P G Martin, E Martínez-González, S Masi, S Matarrese, T Matsumura, F Matthai, P Mazzotta, P McGeehee, A Melchiorri, L Mendes, A Mennella, M Migliaccio, S Mitra, M A Miville-Deschénes, A Moneti, L Montier, G Morgante, D Mortlock, D Munshi, J A Murphy, P Naselsky, F Nati, P Natoli, C B Netterfield, H U Nørgaard-Nielsen, F Noviello, D Novikov, I Novikov, S Osborne, C A Oxborrow, F Paci, L Pagano, F Pajot, D Paoletti, F Pasian, G Patanchon, O Perdereau, L Perotto, F Perrotta, F Piacentini, M Piat, E Pierpaoli, D Pietrobon, S Plaszczynski, E Pointecouteau, A M Polegre, G Polenta, N Ponthieu, L Popa, T Poutanen, G W Pratt, G Prézeau, S Prunet, J L Puget, J P Rachen, M Reinecke, M Remazeilles, C Renault, S Ricciardi, T Riller, I Ristorcelli, G Rocha, C Rosset, G Roudier, M Rowan-Robinson, B Rusholme, M Sandri, D Santos, A Sauvé, G Savini, E P S Shellard, L D Spencer, J L Starck, V Stolyarov, R Stompor, R Sudiwala, F Sureau, D Sutton, A S Suur-Uski, J F Sygnet, J A Tauber, D Tavagnacco, L Terenzi, M Tomasi, M Tristram, M Tucci, G Umana, L Valenziano, J Valiviita, B Van Tent, P Vielva, F Villa, N Vittorio, L A Wade, B D Wandelt, D Yvon, A Zacchei, and A Zonca. Planck 2013 results. VII. HFI time response and beams. *arXiv.org*, pages 1–31, March 2013.
- [60] J A Tauber, H U Nørgaard-Nielsen, P A R Ade, J Amiri Parian, T Banos, M Bersanelli, C Burigana, A Chamballu, D de Chambure, P R Christensen, O Corre, A Cozzani, B Crill, G Crone, O D’Arcangelo, R Daddato, D Doyle, D Dubruel, G Forma, R Hills, K Huffenberger, A H Jaffe, N Jessen, P Kletzkine, J M Lamarre, J P Leahy, Y Longval, P de Maagt, B Maffei, N Mandolesi, J Martí-Canales, A Martín-Polegre, P Martin, L Mendes, J A Murphy, P Nielsen, F Noviello, M Paquay, T Peacocke, N Ponthieu, K Pontoppidan, I Ristorcelli,

- J B Riti, L Rolo, C Rosset, M Sandri, G Savini, R Sudiwala, M Tristram, L Valenziano, M van der Vorst, K van 't Klooster, F Villa, and V Yurchenko. Planck pre-launch status: The optical system. *Astronomy and Astrophysics*, 520:A2, September 2010.
- [61] Levon Pogosian and Alex Zucca. Searching for primordial magnetic fields with CMB B-modes. *Classical and Quantum Gravity*, 35(12):124004, May 2018.
 - [62] Planck 2018-VI. Planck 2018 results. VI. Cosmological parameters. July 2018.
 - [63] C. Rosset, M. Tristram, N. Ponthieu, P. Ade, J. Aumont, A. Catalano, L. Conversi, F. Couchot, B. P. Crill, F.-X. Désert, K. Ganga, M. Giard, Y. Giraud-Héraud, J. Haïssinski, S. Henrot-Versillé, W. Holmes, W. C. Jones, J.-M. Lamarre, A. Lange, C. Leroy, J. Macías-Pérez, B. Maffei, P. de Marcillac, M.-A. Miville-Deschénes, L. Montier, F. Noviello, F. Pajot, O. Perdereau, F. Piacentini, M. Piat, S. Plaszczynski, E. Pointecouteau, J.-L. Puget, I. Ristorcelli, G. Savini, R. Sudiwala, M. Veneziani, and D. Yvon. Planck pre-launch status: High Frequency Instrument polarization calibration. *A&A*, 520:A13+, September 2010.
 - [64] Planck collaboration. Planck intermediate results. XLIX. Parity-violation constraints from polarization data. *Astronomy and Astrophysics*, 596:A110, December 2016.